Dear Prof. Haynes and Reviewers,

We would like to thank the three reviewers for their constructive comments. There are several questions raised, which we will address in the revised version of the manuscript and which will improve the scientific relevance of the paper. In particular, all reviewers asked about the representativeness of the chosen year 2006 and how interannual variation compares to differences between the two hemispheres. We have performed additional simulations and data analysis to discuss this point.

First of all, we would like to set this paper in the current state of knowledge. Several papers comparing single sources such as convection with observations have been published. Most of them are either completely theoretical using educated guesses for spectral distributions, or purely observational; some of them show correlations to proxies of deep convection (e.g. McLandress et al., 2000; Jiang et al., 2004; Jia et al., 2014). There are a few studies which compare distributions in the hot spot regions (Choi et al., 2009, 2012). These studies used an educated guess to define the free parameters governing the spectral case and they confine this guess by the global distribution of variances.

In our paper, for the first time the spectral information by global observations is used to confine the spectral distribution in a CGW model. This is an important advance. The spatial distributions are then used as an additional test. Furthermore, we estimate the relative importance of convective GWs for the momentum budget in different parts of the world. The step by step approach, confining the parameters first and using these for the global distributions again is an important advance in comparison with previous studies. This point will be highlighted in the rewritten introduction.

The educated guess often leads to very small scales of convective waves. Such scales have been corroborated in case studies, but cannot be confined via limb sounding. Our results, however, suggest that the scales seen by the limb sounders and the very short scales form two distinct maxima which both need confinement. In particular, the presented momentum flux and drag estimates clearly show that the longer waves seen by limb sounders carry momentum flux essential for the global circulation.

With current observations (at least such which provide global statistics) we cannot actively sort for different sources. Thus, we can constrain free parameters only for these regions where CGWs dominate. In other regions where CGWs provide only a minor contribution, using scales from a different region of the Earth probably leads to some uncertainties, however only minor ones. The second part of the paper, where we consider global distributions, allows us to estimate the contributions of CGWs to the total GWMF in a global context. This does not mean that we can explain the global distribution, but it means we can identify regions where different sources are required.

A complete explanation by models / parameterizations for all important sources should be our final aim, but it needs confinement of the various individual sources in well defined steps. This is far beyond the scope of a single paper. It is essential to well document the single steps concerning the various sources because in order to use a certain parametrization in e.g. a GCM, it should be confined in a thorough way. This is done here for the Yonsei convective scheme.

There are limitations of the current approach, which are clearly stated in the body of the manuscript and the summary. Overcoming these limitations would require very intensive new studies or even new satellite instruments. This is, however, beyond the scope of the paper.

A detailed reply to the comments and questions of the reviewers is given below. Reviewer

comments are quoted in bold text style, replies are given in normal text style, and changes made are indicated in italic. In addition, all changes are highlighted in the marked PDF manuscript.

Sincerely,
Thai Trinh

Reply on reviewer comments on paper draft: "Tuning of a convective gravity wave source scheme based on HIRDLS observations"

***

Reviewer #1:

General comments:

This work is clearly structured with detailed descriptions of presented figures. Abstract, Introduction and Discussion are of appropriate length and nicely put the topic of this work into the broad context of gravity wave parameterizations and their problems with appropriate references where needed. The paper presents a systematic tuning of the Yonsei Convective Gravity Wave Scheme using observational data. Due to the limitations of observational data such a comparison is not a straight-forward undertaking, but the authors manage to produce new, interesting and useful results by using a unique and ambitious modeling and analysis strategy. Limitations of this approach are discussed as well. Certain aspects of the work need clarification and the language and phrasing should be improved in several paragraphs.

We thank the reviewer for her/his positive comments about the structure as well as for emphasizing the uniqueness of the approach used in our current work.

Specific comments:

1. **Page 34326, Lines 7-8: At first it was not clear to me what "applying a comprehensive observational filter on simulated GWs" entails. Maybe rephrase and say something along the lines of: "The instrument can only see a limited portion of the gravity wave spectrum due to visibility effects, ...ect. ...To allow for a fair comparison of simulated GWs to observations a comprehensive filter is applied to the simulated waves that mimics the instrument limitations."**

   We rephrase as follows:

   The instrument can only see a limited portion of the gravity wave spectrum due to visibility effects and observation geometry. To allow for a meaningful comparison of simulated GWs to observations a comprehensive filter, which mimics the instrument limitations, is applied to the simulated waves.

2. **Page 34326, Line 9: "effects". Can you specify effects on what? It would be helpful to let the reader know right away what effects you will be looking at, i.e. the zonal mean forcing at a certain altitude range.**

   To specify the effects, the sentence is rewritten as follows:

   Results show that spectrum, distribution of momentum flux, and zonal mean forcing of long horizontal scale convective GWs can be successfully simulated by the superposition of three or four combinations of parameter sets reproducing the observed GW spectrum.

3. **Page 34329, Lines following line 5: The introduction has been very clear to this point. Here things become difficult to understand. - Why does tuning based on observations help with producing results that are representative of other years?**

Is this even what you intend to say? I find this sentence confusing. - "adjusting the amplitudes of individual waves while keeping the overall flux the same". Now you are talking about the intermittency factor. But when I read this for the first time, I had no idea what you are referring to or what the idea behind this was. Later on you very nicely introduce the intermittency factor and explain its meaning and consequences. I suggest call it "intermittency factor" here, and say this is an additional tuning parameter that controls the wave amplitude and therefore determines breaking levels. Then it will also be clear why you are mentioning vertical cross sections next. You can leave the detailed explanation for later. - You mention this observational filter but still haven't told us what it is. Please mention briefly what it does. The reader can guess but it's better to just say it explicitly.

Observations of GW momentum flux (GWMF) show similar distributions for different years in terms of e.g. global maps and zonal means (e.g. Ern et al., 2006; Alexander et al., 2008; Ern et al., 2011). Obviously, physical mechanisms like source distributions and wind filtering lead to GW distributions that are typical for each season. We therefore expect that current results are representative of other years.

We add this text to the manuscript:

Although simulations focus on the year 2006, similar convective regions are observed in different years (e.g. Ern et al., 2006; Alexander et al., 2008; Ern et al., 2011) and the current study aims to determine general characteristics of convective GWs by tuning the parameterization based on observations. This will be supported by model-measurement comparison of three consecutive years.

To verify our assumption, we have performed additional analysis and results are shown in Figure A1 in the revised manuscript. In Figure A1, color code shows filtered simulated spectrum and dashed contour lines show the respective observed spectrum at 25 km altitude. These results show that selected scale sets for 2006 generally can reproduce well the observed GWMF spectrum of several other years, except January 2007, which needs further investigation.

Following the suggestion of the reviewer, we rephrase the sentence containing "adjusting the amplitudes of individual waves while keeping the overall flux the same" in a more general formulation:

We also introduce an additional tuning parameter that controls the initial wave amplitude and therefore determines breaking levels. Details about this parameter will be explained later in the paper.

The sentence about the observational filter is rephrased to be more explicit:

Again, the observational filter, which mimics the limitation of the instrument due to visibility effects and observation geometry, is applied to the simulations, and we can investigate the relation between absolute GWMF and GWD.

4. **Page 34330, Line 21: Are ρ_0 and T_0 the density and temperature at the cloud top?**

   Yes, ρ_0 and T_0 are the density and temperature at the cloud top; the text in the revised manuscript is modified accordingly.

5. **Page 34330, Line 16: Do you mean filtering by the background wind when you refer to the vertical propagation condition? No all readers may know what this is. Maybe add a few words for clarification.**

Vertical propagation condition of internal GWs refers to $m^2 > 0$ and $c \neq U$, where m is the vertical wavenumber, c is ground-based phase speed and U is the background wind. In the case study of Song and Chun (2005), m^2 is always positive, thus vertical propagation condition here only refers to critical-level filtering. More details can be seen in the first paragraph, page 112 of Song and Chun (2005).

The sentence is rewritten for clarification as follows:

$|X|^2$ *also represents gravity wave filtering by the background wind during vertical propagation up to the cloud top.*

6. **Page 34330, Line 20: What is the shape of theta(c) as a function of c? I'm curious what equation 2 looks like when you plot theta versus c. Secondly, in the Beres parameterization, for example, there are also assumptions about the shape of the heating in space and time. But in addition to that a sine-shape is assumed for the distribution in the vertical. Does your parameterization assume some kind of vertical shape? If so, what is it?**

First, if we plot θ versus c, we will see that θ has a maximum at the phase speed equaling to c_q and monotonically decreases as $|c - c_q|$ increases. Such a plot is shown in Figure 6a of Song and Chun (2005).

We add this sentence into the manuscript:

The function $\theta(c)$ *has a maximum at the phase speed equaling to* c_q *and monotonically decreases as* $|c - c_q|$ *increases (cf. Fig. 6a in Song and Chun, 2005).*

Second, in the parameterization used in the current work, the vertical configuration of the heating ζ_q is a 2nd order polynomial described by equation (8) in Song and Chun (2005):

$$\zeta_q = \begin{cases} 1 - [(z - z_m)/z_d]^2, & \text{for } z_b \leq z \leq z_t, \\ 0, & \text{elsewhere,} \end{cases}$$

where z_t, z_b are altitudes of cloud top and cloud bottom, respectively; $z_m = (z_t + z_b)/2$, $z_d = (z_t - z_b)/2$.

Parameters z_t, z_b and q_0 are input parameters of the convective source scheme.

7. **Page 34331, Line 1: How do you determine q0? How do you determine cq?**

To define q_0, heating profiles provided by MERRA data are fitted using a second order fit. This is based on the assumption about vertical configuration of the heating in Song and Chun (2005). Cloud top and cloud bottom data from the MERRA data set are used as a first guess for the second order fitting. Results of this second order fit are then used to recalculate top and bottom of the forcing regions. Also, the maximum value of the fitted heating profile between recalculated forcing top and forcing bottom is defined as q_0.

The moving speed c_q is determined as the horizontal background wind averaged below 700mb (Choi and Chun, 2011).

We add this sentence into the manuscript:

The parameters q_0 *and* c_q *as well as the cloud bottom and cloud top height needed to calculate the wave-filtering and resonance factor are determined from MERRA as*

follows: The vertical configuration of the heating is a 2nd order polynomial (cf. Eq. 8 of Song and Chun, 2005). Based on that assumption, heating profiles provided by MERRA data are fitted using a second order fit. Cloud top and cloud bottom data from the MERRA data set are used as a first guess for the second order fitting. Results of this second order fit are then used to recalculate top and bottom of the forcing regions. Also, the maximum value of fitted heating profile between recalculated forcing top and forcing bottom is defined as q_0. The moving speed c_q is determined as the horizontal background wind averaged below 700mb (Choi and Chun, 2011).

8. **Page 34331, Line 6: Can you give a description of the physical meaning of deltax and deltay? Some of the values for your deltax and deltay are so large that they cannot describe convective cells. Convective systems of such scales consist of many smaller convective cells. deltax=4 would be representative of a single convective cell. What scale is it that deltax and deltat describe? Gravity waves are triggered by the individual cells inside such large systems. Therefore, could you better motivate your approach of using these numbers in a parameterization that was intended for individual cells? This really is one of the most central points of your paper and one that I am not quite comfortable with at this point.**

   Convection is parameterized and there is still large uncertainty whether the actual convective parameterization represents the spatial organization of the precipitation (Ricciardulli and Garcia, 2000; Kim et al., 2007). Given that uncertainty, we use the latent heat release values from single grid cells and attribute to these the scales which are best compatible with the GW observations. One advantage of this approach is that it keeps the scheme itself as simple and straight forward as possible.

   The horizontal scale δx and time scale δt used in the convective GW source scheme (Song and Chun, 2005) are free parameters. In previous studies, these parameters have been defined using educated guess. In the current work, these parameters are defined using spectral information from observations. Therefore, we first keep an open mind and estimate δx and δt by adaption to the observed spectrum. A potential physical process related to these δx and δt values will be discussed later in the paper. We added some sentences at this place to clarify the motivation as follows:

   It should be noted that in previous studies the free input parameters δx and δt have been defined using educated guesses. In the current work, these parameters are defined using spectral information from observations. Therefore, we first keep an open mind and estimate δx and δt by adaption to the observed spectrum. A potential physical process related to these δx and δt values will be discussed later in the paper.

   Later on, in Page34335, Line23 of the ACPD manuscript, we discussed that the scales found by our method quantitatively agree well with those found in the convective system studies of Liu and Zipser (2015); Khouider and Moncrieff (2015); Kilpatrick and Xie (2015). Also, in the discussion section (Page 34346, Lines 13-21), the meaning and importance of these found scales are discussed.

9. **Page 34331, Line 7: You are talking about the intermittency factor further down in this paragraph. But selectively sampling the phase speed spectrum also affects the total GWMF. If you didn't use 10, but 20 samples, or 5, - how would you correct for this different number of waves? You somehow have to be sure they are giving you the flux of the whole phase speed spectrum. Can you please comment on this?**

In the current work, simulations are performed using 3-hourly MERRA data for a month. Based on these data, monthly averages are calculated. With this quite large number of events/ snapshots, we expect that the flux of the whole phase speed spectrum is reasonably reproduced. In addition, the spectrum typically has several (even less than 10) very strong peaks and most of the momentum flux is contained in these peaks.

10. **Page 34331, Line 12: Where does the heating depth come from? It appears to be a free parameter just like deltax and deltat. How does the heating depth enter the parameterization?**

    The heating depth is actually calculated by applying a second order fit to the heating profile provided by MERRA data set (please see my reply for the specific comment #7). Also in the reply for the specific comment #7, how the heating depth enters the parameterization is described.

11. **Page 34331, Line 20: What information exactly are you getting from the MERRA latent heat input data? You are assuming deltax and deltat, which wouldn't be resolved anyway because the MERRA grid is too coarse. MERRA can neither resolve the heating depth of individual convective systems. This is a key point that needs clarification.**

    The chief aim of the parameterization is to capture the total amount of rain and the vertical redistribution of water. That should confine the vertical structure of latent heat release. This is the only explicit input we require from MERRA for our study.

    We modify text in the manuscript as follows:

    The vertical profile of latent heat release is taken from three-hourly MERRA (modern-era retrospective analysis for research and applications) assimilated data, which uses a parameterization for convection. The chief aim of the parameterization is to capture the total amount of rain and the vertical redistribution of water. That should confine the vertical structure of latent heat release. This is the only explicit input we require from MERRA for our study. Spatial and temporal scales of the convection are formulated in the CGWs scheme as described above.

12. **Page 34334, Line 4: How can a certain step width optimize computational efficiency? Isn't is more like minimizing the number of different scales that improves computational efficiency?**

    The sentence is rewritten as follows:

    These scales are selected on one hand to cover the whole potential ranges, on the other hand with the appropriate step width to minimize the number of different scales and therefore to improve the computational efficiency.

13. **Page 34335, Lines 22 ff: Yes, different combinations are needed, but how do you know that this has something to do with the hemisphere? If you looked at just one hemisphere but at different years, can you be sure that the best combinations would differ less from year to year for the same hemisphere than they differ between hemispheres? We do not know the uncertainty of these spectra. Is there any way to give an estimate of error bars?**

    We followed the reviewers suggestion and investigated different years both in the observations and the simulations. We have the following key findings:

- There is variation in the vertical wavelength and total strength of GWMF likely associated with the propagation conditions due to the QBO.
- The horizontal wavelength is consistent among different years and shorter for the Northern Hemisphere than for the Southern Hemisphere.
- This latter finding is a source property.
- The consistency between different years shows that this difference is significant.

For details please read appendix A.

14. **Page 34335, Line 25 ff: Would a new paragraph starting at "These scales" be good here? It seems you are now discussing uncertainties in your approach. Maybe also state this explicitly, i.e. new paragraph: then "there are limitations to our approach:" -You say the scales are determined by the regions of deep convection? How is this? For each panel (or simulation) you set them to constant values. I do not understand what you mean here. - I also do not know what "adopted for convective sources" means. My guess is you want to point out the following: You are talking about the observations and how you compare to observations above deep convection. I think what you are trying to say is that there could be other wave sources. But in minimizing the eta function you are using these observations. I would suggest you work on the language of this paragraph and rewrite it because it is not straightforward to understand.**

    And following this, Page 34336 Lines 1-3: I thought you were only looking at deep convection and not considering shallow convection. So what exactly is the concern when applying your parameterization to the whole hemisphere? That you would include shallow convection? Please clarify.

    "These scales" here means "the selected scales". They are selected based on comparison of simulated spectra and respective observed spectra in certain regions, which are defined as regions of deep convection. These regions are shown in Ern and Preusse (2012). In Page 34334 Line 10 we mentioned these regions once. In order to clarify, a global map is included (Figure 1 in this reply, Figure 2 in the revised manuscript), where these regions of deep convection are marked. For the northern hemisphere, three regions of deep convection are demonstrated by three red rectangles. For the southern hemisphere, three regions of deep convection are indicated by three green rectangles.

    After defining the scales using regions of deep convection of each hemisphere, in order to study the importance of CGWs in the global scale, we used these scales to globally run our model and focus our comparisons later to low-latitude areas of the respective hemisphere. This is the meaning of adopting these scales for the convective sources in each hemisphere.

    As the reviewer suggested, we rewrote that paragraph, explicitly stated "There are limitations to our approach:" and move the paragraph to Sect. 3.2 as follows:

    In Sect. 3.1 the free parameters of the convective source scheme were estimated. In this section, we apply these parameters to global-scale simulations in order to estimate the effect of CGWs on the global distribution of GWMF and GW drag. There are limitations to our approach: The selected scales are determined in regions that are likely dominated by GWs that are excited by deep convection (see Fig. 2 for regions of deep convection as identified by Ern and Preusse (2012)). However, in regions which are

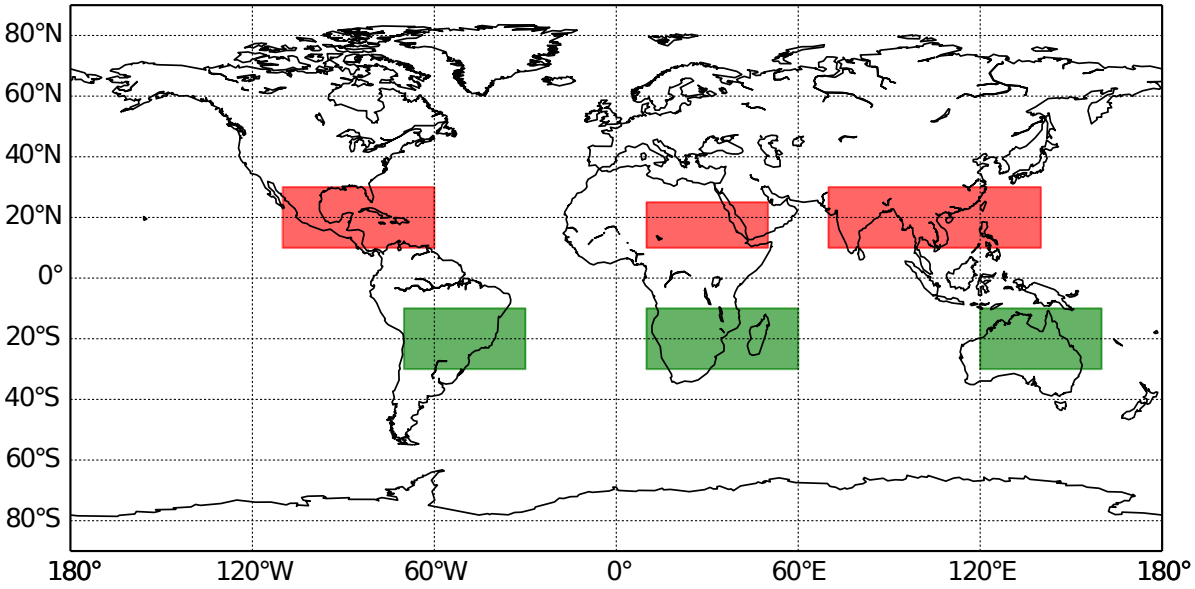

Figure 1: Regions of deep convection. For the northern hemisphere, three regions of deep convection are demonstrated by three red rectangles. For the southern hemisphere, three regions of deep convection are indicated by three green rectangles.

not dominated by one source process, we cannot sort the observed waves according to sources, at least not based on current limb sounding observations. Comparison between observed and modeled spectra thus does not provide a meaningful constraint on the CGW source scheme parameters. Therefore the constraint from the regions of deep convection is the only observational guidance we have and which we consider preferential to a guess. Accordingly, in order to study the importance of CGWs on global scale, the selected sets of δx and δt are used globally for the convective sources for January and July, respectively.

With clarification of the regions of deep convection as well as the rewrite of the paragraph, your questions about Page 34336 Lines 1-3 are also answered.

15. **Page 34337, Line 11: In the previous section (page 34334, line 20) you restrict the HIRDLS data to regions that were previously identified as regions of deep convection. You haven't stated what is shown in Figs 3 and 4, all HIRDLS data or HIRDLS data for regions of deep convection only? Please add this information. If you are comparing to all HIRDLS data: is this necessary? Or could you only look at regions of deep convection as before? If you are comparing to convective regions only: Why would you be so concerned about sources other than convection?**

As mentioned in the reply for comment #14, in order to study the importance of CGWs in the global scale, we we used the scale sets selected for the respective summer hemisphere for performing global runs. In this way, we are able to compare our simulations to full global distributions of HIRDLS observations. To clarify, we added this sentence at Page 34337, Line 6:

It should be noted that observations from HIRDLS shown in Fig. 4 and Fig. 5 contain global data of all regions, not only the regions of deep convection.

Note that in the revised manuscript, since we added one figure, the figure numbering is changed.

The global modeling provides us an estimate of the momentum flux of CGWs. By comparing this to the observed GWMF we can estimate the relative importance of CGWs to the overall momentum flux even in the regions which are dominated by other sources than convection.

16. **Page 34337, Line 20-21: The description of the features in Figures 3 and 4 is careful and good. However, I am not convinced that the differences are solely due to other sources. Your intermittency factor, for example, changes the wave amplitude, the breaking level and could impact the height of the maximum GWMF. And my guess is that GROGRAT introduces some uncertainties as well that could impact the width. Could you comment on this?**

    Yes, the factor α can change the breaking level, impact the height of the maximum GWMF and also can impact the magnitude of GWMF and its vertical gradients. Scales of CGWs were defined based on spectral information from the regions of deep convection, where CGWs dominate. However, the zonal average was calculated globally, including other regions where other sources can be more important. The difference is therefore most likely due to other sources.

    We have some estimates for the errors which GROGRAT could introduce. For example, in an extension of the study of Preusse et al. (2014), GW parameters derived from ECMWF at a low altitude (e.g. 12 km) are used as launch parameters for GROGRAT. With these launch parameters the global distribution is projected to higher altitudes (e.g. 35 km). Comparison of GWMF from GROGRAT ray-tracing calculations and GWMF from ECMWF at that higher altitude shows generally good agreement and the differences are much smaller than the effects we discuss here. This means that GROGRAT provides results comparable to a model that explicitly resolves the GWs. Though these extended studies have not been published yet, they make us confident that the uncertainties of the ray-tracing technique are minor compared to other effects discussed here.

17. **Page 34339, Lines 13-14: Why does the wind maximum affect Q this strongly? When you discuss the observational filter, there was no mentioning of wind effects. Could you add a sentence saying how the wind affects Q?**

    The wind influences the vertical wavelength and via this enters the observational filter. Whether or not there is a difference between Q and P depends on the vertical wavelength of those waves which dissipate and deposit momentum. The vertical wavelength separating the saturated and unsaturated part of the spectrum is larger at higher altitudes. In case of similar Q and P critical level filtering is less important. We reformulate the sentences as follows:

    In both Fig. 4e and Fig. 4d, strong dissipation can be seen for a wind maximum at 40-45 km altitude and 20°S, which is located above the strongest sources. The maximum is similar strong in Q and in P indicating that observational filter effects are less important. This is the case for waves with vertical wavelengths longer than the short-wavelength edge of the observational filter. This also means that critical level filtering is not relevant at this point. For longer vertical wavelengths, dissipation may be reached just by the exponential amplitude growth which compensates the decrease of atmospheric density. This is particularly likely in regions where GW amplitudes are large already at excitation level. The net drag in Fig. 4d is low indicating that waves

from both propagation directions contribute, which is compatible with saturation by amplitude growth. A small preferential net drag in this case is caused by a preferential direction in GWMF. Similar strong dissipation can be seen at the same altitude range at about 20°N in Fig. 5d and Fig. 5e. Here the preference in propagation direction and net drag are considerably stronger. This dissipation in the upper stratosphere is important for the driving of the SAO in the tropics (cf. discussion in Ern et al., 2015).

Note that in the revised manuscript, the figure numbering is changed.

Technical corrections:

Page 34326, Lines 13 & 14: "flux" is singular, "are" is plural.
Text has been modified as follows: are → is

Page 34327, Line 22: Suggest MF1 → "MF1" for this first time.
Modified as suggested.

Page 34328, Line 29: ", which" →"that"

Modified as suggested.

Page 34329, Line 3: "which fit best to the" → "which best fit the"

Modified as suggested.

Page 34329, Line 6: I don't think "grounded" is a good word. Suggest "based on" or "informed by".

"grounded on" → "based on"

Page 34329, Line 8: you are in fact showing meridional, not zonal cross sections.

"zonal cross sections" → "zonal mean cross sections"

Page 34330, Line 20: shaped → shape

Rewritten as shown in the revised manuscript.

Page 34334, Line 7: by → for

Modified as suggested.

Page 34335, Line 22: "northern" and "Southern".

"northern" → "Northern"

Reviewer #2:

General comments:

The present manuscript constitutes an extension of the results described in a very recent Atmos. Meas. Tech (2015) paper, by Trinh et al. A correct parameterization of GWs still represents a great challenge. Here, simulated GWs taking into account different sets of spatial and temporal scales to represent convection sources are generated and propagated following trajectories calculated from the GROGRAT model. In order to compare the simulations with HIRDLS observations, a comprehensive observational filter is applied. The observed spectra reproduce the spectral shape and location of the peak by a combination of four scale sets. The contribution of these waves to the momentum balance is evaluated by calculating zonal mean cross sections of absolute GWMF and its vertical gradients and comparing them to respective observed quantities. Several features regarding wave propagation and visibility in the middle atmosphere as well as zonal average of filtered simulated GWMF and wave drag are discussed against observed GWMF. The horizontal distributions of absolute unfiltered and filtered GWMF are also presented in this work. A good agreement with observed horizontal distributions in the structure as well as the magnitude is claimed. Main convection hot spots are reproduced. The GWMF spectra in terms of zonal phase speed and latitude are shown.

In this manuscript, the scientific results and conclusions are presented in a clear and well-structured way and the results and figures, well presented too. As the authors finally say, I agree that due to the limitations of current global observations, the synergetic use of physics based models, observational filter and observations using both absolute values of GWMF and its vertical gradient is very important to infer the true properties of GWs in the atmosphere. Nevertheless, my main concern is related to the consequences on the final results, after the chain of implicit and explicit accumulated assumptions and hypothesis involved throughout these calculations.

We thank the reviewer for the generally positive attitude on the paper and the positive comments on structure and quality. The reviewer pointed out several interesting points, which will be discussed below.

Some of the reviewer comments suggest that we need to better distinguish our work from previous studies and show the advance of our approach. We therefore inserted the following paragraph in the introduction:

Till recently, several papers comparing single sources such as convection with observations have been published. Most of them are either completely theoretical using educated guesses for spectral distributions, or purely observational; some of them show correlations to proxies of deep convection (e.g. McLandress et al., 2000; Jiang et al., 2004; Jia et al., 2014). There are a few studies which compare distributions in the hot spot regions (Choi et al., 2009, 2012). These studies used an educated guess to define the free parameters governing the spectral distribution and confine this guess by the global spatial distribution of GW variances. In our paper, for the first time, the spectral information by global observations is used to confine the spectral distribution in a CGW model. The spatial distributions are then used as an additional test. Furthermore, we estimate the relative importance of convective GWs for the momentum budget in different parts of the world. The step by step approach, confining the parameters first and using these for the global distributions again distinguishes this paper from previous studies.

Using a number of different sources and different and complementary observations is, of course, a major aim for the community. At the present stage of research, however, it cannot

be expected from a single study.

Specific points mentioned by the reviewer:

1. **The 2D restriction of cloud parameterization and the Yonsei 3-layer model scheme. How resistant may be expected to be the filtered and unfiltered GWMF distributions to different schemes for convection and other years, taking into account the interanual variability and climatological departures (e.g., ENSO) from 2006?**

   From the variation of the two free model parameters in Figure 1 (in the manuscript) it can be seen that these free parameters affect mainly the horizontal wavelength. The vertical wavelength distribution is largely determined by the theoretical conception of the model, namely the resonance factor. We hence use the measured spectra to a) gain information on the horizontal scale, which is not determined by the model conception, but b) also to validate the vertical wavelength spectrum. This is a corroboration of the model assumptions. The comparison of the spectrum hence is a confirmation that the basic assumptions of the model describe reality well, at least in a statistical sense.

   We add these sentences into Sect. 3.1 of the manuscript:

   We hence use the observed spectra to a) gain information on the horizontal scale, which is not determined by the model conception, but b) also to validate the vertical wavelength spectrum. This is a corroboration of the model assumptions. The comparison of the spectrum hence is a confirmation that the basic assumptions of the model describe reality well, at least in a statistical sense.

   Furthermore, to verify the scale sets selected using observations of 2006 in climatological conditions of other years, we performed additional analysis. These results were discussed in reply #3 for the reviewer #1 and included in the paper in appendix A.

   As shown by Figure A1 of the revised manuscript, the selected scale sets can generally reproduce the observed GWMF spectra of other climatological conditions well. In particular, the interanual variability in the Northern Hemisphere, which is likely related to the QBO, is very well captured.

2. **The exclusion of sources other than convection, mainly orographic sources at mountaineous regions, may represent an important restriction. The importance of penetration of mountain waves into the middle atmosphere and aloft as well as their vertical flux of energy and zonal momentum is broadly accepted (e.g. Preusse et al 2014 and referenes therein). The derivation of eq. (3) for GWMF assumes a single (or prevailing) monochromatic wave and the mid freuencey (hydrostatic) approximation. CGW is a multiscale problem. On the other hand, the GWMF strictly due to mountain waves might be better described by this equation than the contribution due to convection, as far as a common feature in mountain waves spectral analyses is the assumption of one or two prevailing modes of oscillation and a relatively small amount of energy distributed along the remaining spectrum.**

   In the first step we confine the free parameters of the CGW scheme. This is based on the spectral information. For this, we need regions where CGWs dominate. So, for this we may ask whether mountain waves (MWs) are important in these regions? The answer is no: Spatial (e.g. Spang et al., 2002; Jiang et al., 2004) as well as temporal correlations (e.g. Preusse and Ern, 2005; Jia et al., 2014) indicate in the considered regions a clear

dominance of convective GW excitation. The physical reason is the weak winds, or even a wind reversal between troposphere and stratosphere, in the subtropics. As a result, the upward propagation of MWs is suppressed. It should be further noted that MWs with zero ground-based phase speed, if important, are normally clearly visible in the spectrum as well as in the vertical profile of GWMF (cf. Preusse et al., 2009). Our own data hence confirm the non-importance of mountain waves in the subtropics.

In the second step we consider the importance of CGWs on global scale. Here we clearly see that in the winter hemisphere at mid and high latitudes other sources are more important. In order to simulate the whole global distribution, we need a representation of all relevant sources. This, however, exceeds the scope of this paper. It should be noted, in particular, that this would require waves from jets and fronts, concepts of which are just being developed.

The reviewer concerns about using monochromatic wave assumption for a wide range spectrum of CGWs. This assumption has been investigated in the study of Lehmann et al. (2012). In Lehmann et al. (2012), WRF simulations of convective waves are used to compare spectra obtained from 2D Fourier transform with a single-wave approach based on small-volume sinusoidal fits. Using an area containing a typhoon and its spiral band, a wide range of convective scales is represented. It turns out that in a statistical sense both approaches agree well, i.e. by many different single waves covering small areas almost the same spectrum is generated as by a Fourier transform of the whole region. We thus expect, that no larger distortions of the spectrum are generated by the chosen approach. In addition, the modeling approach is based on a number of discrete waves, which enhances compatibility between the two approaches.

We add these sentences into the manuscript after Equation (3):

Although Eq. (3) is based on monochromatic wave assumption while CGWs are a multiscale problem, it was shown that in a statistical sense, spectra of CGWs obtained from 2D Fourier transform can be well reproduced using a single-wave approach (Lehmann et al., 2012). Furthermore, our modeling approach is based on a number of discrete waves, which enhances compatibility between the two approaches. We thus expect, that no larger distortions of the spectrum are generated by the chosen approach.

3. **As the authors clearly state, the adoption of parameter choices determined by deep convection regions for the entire respective hemisphere represents one important limitation of this approach.**

   This is of course a limitation. However, with current instruments we cannot sort waves into individual sources. It is still better to use some measured constraint than the alternative, purely educated guesses. We add these following sentences in the revised manuscript in Sect. 3.2:

   However, in regions which are not dominated by one source process, we cannot sort the observed waves according to sources, at least not based on current limb sounding observations. Comparison between observed and modeled spectra thus does not provide a meaningful constraint on the CGW source scheme parameters. Therefore the constraint from the regions of deep convection is the only observational guidance we have and which we consider preferential to a guess.

4. **The absolute value of filtered GWMF is lower, in comparison with this observed magnitude, which, as discussed above can be explained by a lack of other sources**

different from convection. In addition to this, as the authors state the geographical distribution due to the effect of the observational filter may be different at different regions.

The by far larger effect should be the presence of other sources. At high winter latitudes, CGWs contribute only a minor part of the total GWMF. This can be seen from the unfiltered GWMF values as well. Shorter scale CGWs (MF1) cannot be constrained by limb sounders and may exist in addition. Their contribution cannot be quantified. We add these sentences to Sect. 3.2:

At high winter latitudes, CGWs contribute only a minor part of the total GWMF. This can be seen from the unfiltered GWMF values as well.

5. **The comparison of the unfiltered results with GWMF obtained from other limb instruments as GPR radio occultations, could be useful.**

   All instruments have observational limitations. The visibility due to radiative transfer and retrieval for GPS-RO is almost identical with the one of IR limb sounders. Many GPS-RO studies are, however, further limited by the removal of the background in terms of vertical detrending. Comparisons with other instruments make sense, if and only if they include the observational filter. Unfortunately, very few in-detail discussions of the complete observational filter for GPS-RO exist. Such a work should be subject to a separate technical paper and needs detailed consideration of the observation geometry.

6. **In my opinion, in Figures 5-8, besides the agreement in the detection of he hotspots, the considerable differences between subfigures a, c and e, should be better explained and discussed.**

   Qualitatively we have discussed this: other sources. Quantitatively one would need models for these other sources, e.g. mountain waves, jets and fronts ... However, there may be sources, which we even often do not discuss at all. That would provide a wide field for speculations, but is not what we like to reach in terms of robust results. Our major aim in the second part of the paper is not to explain the global distribution, but identify regions where different sources are required. A better agreement between observations and simulations for the complete picture should be the final aim, but it requires other model sources and is far beyond the scope of a single paper.

Reviewer #3:

General comments:

This paper describes an application of the Song and Chun, 2005 convective gravity wave source parameterization using the GROGRAT ray-tracing model, an observational filter consistent with limb sounders (e.g. HIRDLS) with a focus on January and July 2006 (using MERRA Reanalysis data). The papers aim is to better understand the confounding influence of convective sources (and their concomitant wave spectra) and the filtering of the background winds on the climatology of observed small scale gravity waves. The study represents a bold attempt in using a combination of source parameterizations and (ray-tracing) modelling (including dissipation mechanisms) to gain additional useful information in light of the current paucity of suitable (satellite) observations.

The paper has about the right number of suitable figures for a paper of this type and restates briefly all the main conclusions in the abstract. It is generally well written although would benefit from further proof reading for grammar from the native english speaking co-authors.

I suggest that some of the analysis be redone, or further supplementary material added, to examine for the influence of the unique meteorological conditions occurring during the NH winter stratosphere during January 2006. Other similar studies have also made similar use of data, without mention of anomalous filtering effects during this time. Following an adequate addressing of the main points I recommend publication.

Comments

- **There does not seem to be a mention of filtering effects associated with the SSW occurring mid to late January 2006. This event would highlight differences between the NH and SW winters shown. In this respect, why was 2006 chosen? Should some of the conclusions be revised in the light of this? Perhaps another NH HIRDLS-observed winter should be examined for a comparison. Or if the authors are planning to show SSW filtering effects in another paper, they should examine another January year in the present study (e.g. Jan, 2007). GW filtering (as observed by HIRDLS) of this event was reported in Wright et al., 2010, 10.1029/2009JD011858**

  Following the reviewer's comment, we analyzed the simulated spectra for NH summer and SH summer of other years. Results are shown in Figure A1 of the revised manuscript. Detailed discussions are presented in the appendix of the revised manuscript (cf. also reply #3 to reviewer #1 and reply #1 to reviewer #2). As shown, the QBO signal is captured by our simulations. However, influence of the SSW seems to be very minor. This is likely related to the fact that CGWs dominate in the tropics and subtropics, where the QBO is. The influence of CGWs on the QBO is therefore expected to be significant. The SSW occurs in the polar region, where the contribution of CGWs is much less important. This less importance was discussed in the manuscript.

- **A comparison of observations of GWs and GW parameterization employed in GCMs showed a marked difference in the vertical attenuation of GWMF (figure 3 of Geller et al, 2013, 10.1175/JCLI-D-12-00545.1). These differences were in part attributed to the observational window effects apparent in the satellite derived data (resulting in a faster drop-off in GWMF in observations as compared**

to models). It would be good to show if this effect is captured after applying the observational filter used in the present paper.

In the study of Geller et al., 2013 (G13 hereafter), vertical gradients in GWMF are compared between models and satellite observations. Considerable differences were found with the observations showing much stronger vertical gradients on global average. Differences were attributed to the fact that the observations see only a limited part of the GW spectrum, and vertical gradients could be much weaker in parts of the spectrum not seen by the instruments.

Because the G13 comparison was carried out on global averages, this comparison was based on the global distribution of GWs including all GW sources. Comparison with our simulations focusing on CGWs only would therefore be of only limited use. As can be seen from Figs.3b,c and Figs.4b,c (in the ACPD paper) even in the subtropics where CGWs dominate, on zonal average there are considerable differences between zonal average GWMF observed by HIRDLS and zonal average GWMF from our simulations. This indicates that even in the subtropics, on zonal average there is a countable contribution of GWs from sources other than the deep convective sources described by our simulations. We are therefore afraid that this comparison of filtered and unfiltered GWMF vertical gradients would involve considerable uncertainties and not be very robust.

Other comments:

(34330, L19) eq 2 does not describe a Gaussian, although it is derived from one in Song and Chun, 2005.

The diabatic forcing is assumed to be a Gaussian-shaped function, but not the diabatic source function. This sentence was not carefully written. We correct this sentence in the revised manuscript as follows:

$\theta(c)$ *is the diabatic source function, which is described as follows:*

(34331, L18) "larger"

Modified as suggested.

(34336, L17) "ray-tracing calculations"

Modified as suggested.

(34336, L21) The simulated "momentum flux" is shown in figures 3a and 4a, but how is this diagnosed. As previously mentioned, saturation mechanisms including e.g. radiative damping are used to limit the amplitude of rays in GROGRAT, but how is this calculated to produce the absolute GWMF shown? An equation or reference would be good in support of this.

The simulated "momentum flux" (F_{ph}) shown in figures 3a and 4a (in the ACPD paper) is calculated as: $F_{ph} = \sqrt{F_{px}^2 + F_{py}^2}$, where F_{px} and F_{py} are GWMF components in zonal and meridional direction, respectively. F_{px} and F_{py} are results of the ray-tracing calculations (output parameters of GROGRAT). More details about radiative damping calculation in GROGRAT can be found in papers about this model, particularly in (Marks and Eckermann, 1995).

Following the reviewer's suggestion, we add this sentence into the manuscript:

Unfiltered GWMF shown in Fig. 4a and Fig. 5a is calculated as: $F_{ph} = \sqrt{F_{px}^2 + F_{py}^2}$, *where* F_{px} *and* F_{py} *are GWMF components in zonal and meridional direction, respectively, as determined from the ray-tracing calculations.*

Note that the figure numbering is changed.

(34337, L3) Not sure I see stronger reductions in GWMF at and below the tropopause. Also, "stronger" than what in particular?

We remove that sentence in the revised manuscript.

(34337, L10) Suggest "better match at low latitudes. At mid and high latitudes HIRDLS observations indicate an enhancement, likely due to other sources."

Modified as suggested.

(34337, L20) The authors suggest the tropical differences seen between HIRDLS and the filtered GWMF are due to other GW sources. I am not convinced by this. Can the authors describe how the existing convective GW source parameterization formulation could lead to an underestimate in tropical GWMF at low altitudes between 3b,c and 4b,c?

The reviewer has a point that the current text reads as simply shifting all differences to "other sources". We will replace this statement:

The weaker and narrower peak in the simulations could indicate that deep convection is spread over a wider latitude range than simulated in MERRA or that we need to revisit the forcing efficiency. However, there is also indication from radiosonde and ground-based measurements (e.g. Leena et al., 2010; Pramitha et al., 2015) and modeling (e.g. Preusse et al., 2014) indicating that related to regions of deep convection GWs are excited around the tropopause. Details of that GW excitation are not fully understood, but they are presumably associated with the shear and strong buoyancy change present at these altitudes. These waves seem to be less focused to the convective regions and produce a substantial background outside the selected convection regions used for the spectra (cf. Fig. 4c and Fig. 5c) and thus potentially become important in the zonal means.

Note that the figure numbering is changed in the revised manuscript.

(34338, L21) I am not sure of this attribution statement: vertical gradients in wind are located with regions of div_F. The ray-tracing scheme also allows for horizontal propagation and so horizontal and vertical gradients in zonal wind may be associated with div_F. Furthermore, features in the upper tropical stratosphere (e.g. 4d) cannot be explained by a statement like, "positive drag is found in regions of positive wind shear", as in that example the opposite would appear true. Perhaps the authors might like to mention the combination of horizontal propagation as well as dissipative processes not including critical layer filtering, which could better account for the sizeable drag features in the tropical mid to upper stratosphere.

The reviewer is correct that we need to better distinguish between different altitude regions in the atmosphere where different physical processes are responsible for the saturation. At lower altitudes mainly short vertical wavelength waves saturate. At these altitudes we find strong influence of the vertical winds. At higher altitudes there is a dominance of longer vertical wavelengths and saturation is caused chiefly by amplitude growth. In the new text we will clearly separate these two regions. In addition, the vertical wavelength aspect is discussed where we discuss Q and P. So for the lower altitudes the text now reads:

In the tropics (15°S-15°N), in the lower and mid stratosphere (i.e. up to about 35 km) drag is exerted in regions of vertical wind shear. There we find positive drag for positive shear and

negative drag for negative shear as expected for the driving of the QBO.

and further down in the text:

In Fig. 4e the U-shaped structure is much less pronounced in comparison with Fig. 4d, which indicates that the drag is exerted when the waves attained very short vertical wavelength and are already removed by the observational filter from Q. Such short vertical wavelengths would also mean that critical level filtering is an important process in this region.

The text for the higher altitudes now reads:

In both Fig. 4e and Fig. 4d, strong dissipation can be seen for a wind maximum at 40-45 km altitude and 20° S, which is located above the strongest sources. The maximum is similar strong in Q and in P indicating that observational filter effects are less important. This is the case for waves with vertical wavelengths longer than the short-wavelength edge of the observational filter. This also means that critical level filtering is not relevant at this point. For longer vertical wavelengths, dissipation may be reached just by the exponential amplitude growth which compensates the decrease of atmospheric density. This is particularly likely in regions where GW amplitudes are large already at excitation level. The net drag in Fig. 4d is low indicating that waves from both propagation directions contribute, which is compatible with saturation by amplitude growth. A small preferential net drag in this case is caused by a preferential direction in GWMF. Similar strong dissipation can be seen at the same altitude range at about 20° N in Fig. 5d and Fig. 5e. Here the preference in propagation direction and net drag are considerably stronger. This dissipation in the upper stratosphere is important for the driving of the SAO in the tropics (cf. discussion in Ern et al., 2015).

Note that the figure numbering is changed in the revised manuscript.

Also, we state precisely how we calculate the zonal drag. We add this information into the manuscript in Sect. 3.2:

We calculate the drag by calculating the vertical change of zonal momentum flux along the ray. In this way the calculations take into account wave dissipation and horizontal refraction but do not cause a spurious acceleration where GWs just propagate horizontally out off a region where we calculate the vertical gradient.

(34339, L9) suggest moving the word 'only', "The vertical gradient Q only considers the dissipation caused ". The authors might like to consider further describing the differences expected between P and Q. Superficially, the difference comes down to the non-commutativity between the observational filter and the (vertical contribution to the) divergence operator, but the reader will most probably not know what this difference ought to be. Another sentence or two highlighting these differences would be a good idea.

The word 'only' is moved as suggested. We add this sentence for a better clarification:

This also means that dissipation of waves which are not seen by the instrument is not taken into account in Q even though these waves exert real drag and are taken into account in calculating X.

Also, we add these sentences before Eq. (7):

The closest similarity to observed potential drag is provided by P, which takes into account reduction of observed GWMF both by dissipation and by the fact that waves are moving out of the observational filter. In order to distinguish between these two processes we introduce a further quantity which shows only the true dissipation we observe.

(34340, L1) Suggest "As mentioned in Sect. 2.1, further tuning is achieved by reducing the launch amplitude by a factor of $1/\alpha$ and simultaneously multiplying the number of launched rays by a factor of α. In this study α is chosen to be 5."

Modified as suggested.

(34340, L5) Presumably changing α can shift the relative height of saturation higher or lower, depending on how much wave energy is shared within a given wavenumber band. This was mentioned earlier, so I suggest the following; "can affect GWMF aloft, shifting the saturation level to different altitudes."

Modified as suggested.

(figures 3-8) Please mention MERRA data in captions.

Modified as suggested.

(figure 3 caption) presumably the y-axis shows -1/rho*...to be consistent with equations 5-7.

Modified as suggested.

References

Alexander, M. J., Gille, J., Cavanaugh, C., Coffey, M., Craig, C., Dean, V., Eden, T., Francis, G., Halvorson, C., Hannigan, J., Khosravi, R., Kinnison, D., Lee, H., Massie, S., and Nardi, B. (2008). Global estimates of gravity wave momentum flux from High Resolution Dynamics Limb Sounder (HIRDLS) observations. *J. Geophys. Res.*, 113.

Choi, H. J. and Chun, H. Y. (2011). Momentum flux spectrum of convective gravity waves. Part I: An update of a parameterization using mesoscale simulation. *J. Atmos. Sci*, 68:739–759.

Choi, H.-J., Chun, H.-Y., Gong, J., and Wu, D. L. (2012). Comparison of gravity wave temperature variances from ray-based spectral parameterization of convective gravity wave drag with AIRS observations. *J. Geophys. Res.*, 117.

Choi, H.-J., Chun, H.-Y., and Song, I.-S. (2009). Gravity wave temperature variance calculated using the ray-based spectral parameterization of convective gravity waves and its comparison with Microwave Limb Sounder observations. *J. Geophys. Res.*, 114.

Ern, M. and Preusse, P. (2012). Gravity wave momentum flux spectra observed from satellite in the summertime subtropics: Implications for global modeling. *Geophys. Res. Lett.*, 39.

Ern, M., Preusse, P., Gille, J. C., Hepplewhite, C. L., Mlynczak, M. G., Russell III, J. M., and Riese, M. (2011). Implications for atmospheric dynamics derived from global observations of gravity wave momentum flux in stratosphere and mesosphere. *J. Geophys. Res.*, 116.

Ern, M., Preusse, P., and Riese, M. (2015). Driving of the sao by gravity waves as observed from satellite. *Ann. Geophys.*, 33(4):483–504.

Ern, M., Preusse, P., and Warner, C. D. (2006). Some experimental constraints for spectral parameters used in the Warner and McIntyre gravity wave parameterization scheme. *Atmos. Chem. Phys.*, 6:4361–4381.

Jia, J. Y., Preusse, P., Ern, M., Chun, H.-Y., Gille, J. C., Eckermann, S. D., and Riese, M. (2014). Sea surface temperature as a proxy for convective gravity wave excitation: a study based on global gravity wave observations in the middle atmosphere. *Ann. Geophys.*, 32(11):1373–1394.

Jiang, J., Wang, B., Goya, K., Hocke, K., Eckermann, S., Ma, J., Wu, D., and Read, W. (2004). Geographical distribution and interseasonal variability of tropical deep convection: UARS MLS observations and analyses. *J. Geophys. Res. Atmos.*, 109.

Khouider, B. and Moncrieff, M. W. (2015). Organized convection parameterization for the ITCZ. *Journal of the Atmospheric Sciences*, 72(8):3073–3096.

Kilpatrick, T. J. and Xie, S.-P. (2015). ASCAT observations of downdrafts from mesoscale convective systems. *Geophys. Res. Lett.*, 42(6):1951–1958.

Kim, S.-Y., Chun, H.-Y., and Baik, J.-J. (2007). Sensitivity of typhoon-induced gravity waves to cumulus parameterizations. *Geophys. Res. Lett.*, 34.

Leena, P., Venkat Ratnam, M., and Krishna Murthy, B. (2010). Inertia gravity wave characteristics and associated fluxes observed using five years of radiosonde measurements over a tropical station. *J. Atm. Sol.-Terr. Phys.*, 84-85:37–44.

Lehmann, C. I., Kim, Y.-H., Preusse, P., Chun, H.-Y., Ern, M., and Kim, S. Y. (2012). Consistency between Fourier transform and small-volume few-wave decomposition for spectral and spatial variability of gravity waves above a typhoon. *Atmos. Meas. Tech.*, 5(7):1637–1651.

Liu, C. and Zipser, E. J. (2015). The global distribution of largest, deepest, and most intense precipitation systems. *Geophys. Res. Lett.*, 42(9):3591–3595.

Marks, C. J. and Eckermann, S. D. (1995). A three-dimensional nonhydrostatic ray-tracing model for gravity waves: formulation and preliminary results for the middle atmosphere. *J. Atmos. Sci.*, 52:1959–1984.

McLandress, C., Alexander, M. J., and Wu, D. L. (2000). Microwave Limb Sounder observations of gravity waves in the stratosphere: A climatology and interpretation. *J. Geophys. Res.*, 105(D9):11947–11967.

Pramitha, M., Venkat Ratnam, M., Taori, A., Krishna Murthy, B. V., Pallamraju, D., and Vijaya Bhaskar Rao, S. (2015). Evidence for tropospheric wind shear excitation of high-phase-speed gravity waves reaching the mesosphere using the ray-tracing technique. *Atmos. Chem. Phys.*, 15:2709–2721.

Preusse, P., Eckermann, S. D., Ern, M., Oberheide, J., Picard, R. H., Roble, R. G., Riese, M., Russell III, J. M., and Mlynczak, M. G. (2009). Global ray tracing simulations of the SABER gravity wave climatology. *J. Geophys. Res.*, 114.

Preusse, P. and Ern, M. (2005). Indication of convectively generated gravity waves observed by CLAES. *Adv. Space Res.*, 35:1987–1991.

Preusse, P., Ern, M., Bechtold, P., Eckermann, S. D., Kalisch, S., Trinh, Q. T., and Riese, M. (2014). Characteristics of gravity waves resolved by ECMWF. *Atmos. Chem. Phys.*, 14(19):10483–10508.

Ricciardulli, L. and Garcia, R. R. (2000). The excitation of equatorial waves by deep convection in the NCAR community climate model (CCM3). *J. Atmos. Sci.*, 57:3461–3487.

Song, I. S. and Chun, H. Y. (2005). Momentum flux spectrum of convectively forced internal gravity waves and its application to gravity wave drag parameterization. Part I: theory. *J. Atmos. Sci.*, 62:107–124.

Spang, R., Eidmann, G., Riese, M., Offermann, D., Preusse, P., Pfister, L., and Wang, P.-H. (2002). CRISTA observations of cirrus clouds around the tropopause. *J. Geophys. Res.*, 107.

Manuscript prepared for Atmos. Chem. Phys.
with version 2015/04/24 7.83 Copernicus papers of the LaTeX class copernicus.cls.
Date: 24 March 2016

Tuning of a convective gravity wave source scheme based on HIRDLS observations

Q. T. Trinh[1], S. Kalisch[1], P. Preusse[1], M. Ern[1], H.-Y. Chun[2], S. D. Eckermann[3], M.-J. Kang[2], and M. Riese[1]

[1]Institute of Energy and Climate Research, Stratosphere (IEK-7), Forschungszentrum Jülich, Jülich, Germany
[2]Laboratory for Atmospheric Dynamics, Department of Atmospheric Sciences, Yonsei University, South Korea
[3]Space Science Division, Naval Research Laboratory, Washington DC, USA

Correspondence to: Q. T. Trinh (t.trinh@fz-juelich.de)

Abstract. Convection as one dominant source of atmospheric gravity waves (GWs) has been in focus of investigation over recent years. However, its spatial and temporal forcing scales are not well known. In this work we address this open issue by a systematic verification of free parameters of the Yonsei convective GW source scheme based on observations from the High Resolution Dynamics Limb Sounder (HIRDLS). ~~Observational constraints are taken into account by applying a comprehensive observational filteron the simulated GWs~~The instrument can only see a limited portion of the gravity wave spectrum due to visibility effects and observation geometry. To allow for a meaningful comparison of simulated GWs to observations, a comprehensive filter, which mimics the instrument limitations, is applied to the simulated waves. By this approach, only long horizontal scale convective GWs are addressed. Results show that ~~effects of~~ spectrum, distribution of momentum flux, and zonal mean forcing of long horizontal scale convective GWs can be successfully simulated by the superposition of three or four combinations of parameter sets reproducing the observed GW spectrum. These selected parameter sets are different for northern and southern summer. Although long horizontal scale waves are only part of the full spectrum of convective GWs, the momentum flux of these waves ~~are~~ is found to be significant and relevant for the driving of the QBO. The zonal momentum balance is considered in vertical cross sections of GW momentum flux (GWMF) and GW drag (GWD). Global maps of the horizontal distribution of GWMF are considered and consistency between simulated results and HIRDLS observations is found. The latitude dependence of the zonal phase speed spectrum of GWMF and its change with altitude is discussed.

1 Introduction

Gravity waves (GWs) significantly impact global circulations by accelerating or decelerating the background wind while dissipating or breaking (e.g., McLandress, 1998; McIntyre, 1998; Kim et al., 2003; Alexander et al., 2010). For example, GWs are important in driving the quasi-biennial oscil-

lation (QBO) (e.g., Dunkerton, 1997; Ern and Preusse, 2009; Alexander and Ortland, 2010; Evan et al., 2012; Ern et al., 2014; Kim and Chun, 2015) and the semiannual oscillation (SAO) (Ern et al., 2015). Moreover, they are assumed to be the main driver of the summer-time branch of the stratospheric Brewer-Dobson circulation (Alexander and Rosenlof, 2003; Fritts and Alexander, 2003) and play a significant role in wind reversals in the mesosphere and lower thermosphere (Lindzen, 1981; Matsuno, 1982; Ern et al., 2013).

GWs are generated by different sources such as orography, convection or spontaneous adjustment of jet streams. In our work, we will focus on convectively generated GWs. Convection excites GWs via diabatic forcing by latent heat release and has long been accepted as one of the most prominent sources, in particular at low latitudes. However, convection itself is parameterized in large-domain models and global models. Even if part of the GW spectrum is resolved, physics assumptions and mathematical formulation of the convective parameterization influence the characteristics of the excited GWs (Kim et al., 2007; Preusse et al., 2014).

In order to represent in global models the important contribution of convectively forced GWs to large-scale circulations, several parameterizations of GWD induced by cumulus convection have been developed (e.g., Rind et al., 1988; Kershaw, 1995; Chun and Baik, 1998, 2002; Beres et al., 2004; Song and Chun, 2005). In this paper we focus on the convective GW source (CGWS) scheme of Song and Chun (2005). In this CGWS scheme, the spatial scale δx and the temporal scale δt of the diabatic forcing are free tunable parameters. These scales δx and δt cannot be determined from theory. Generally, there are two approaches to define these parameters: (1) forward estimation assuming typical scales of clouds or convective systems or (2) by comparing the resulting GW distributions with observations. The primary scale set "MF1" of the Yonsei CGWS scheme (Song and Chun, 2005) has $\delta x = 5$ km and $\delta t = 20$ min. These scales are selected based on mesoscale simulations conducted by Song et al. (2003). The primary scale set MF1 shows good agreement with GW temperature variance (GWTV) from Microwave Limb Sounder (MLS) observations on board the Upper Atmosphere Research Satellite (Choi et al., 2009) and with GW momentum flux from three-dimensional mesoscale simulations (Choi and Chun, 2011). However, MF1 underestimates the GWTV observed by Atmospheric Infrared Sounder (AIRS) on board the Aqua satellite, and therefore an additional scale set MF2 ($\delta x = 25$ km, $\delta t = 60$ min) was added (Choi et al., 2012). GWTV given by the combination of MF1 and MF2 matches AIRS observations well in both horizontal distribution and magnitude. Nevertheless, this combination cannot explain the GW spectrum observed by HIRDLS, which peaks at longer horizontal wavelength of about 600 km and vertical wavelength of about 10 km (Ern and Preusse, 2012). A possible reason is that MF1 and MF2 do not describe the presence of large-scale convective systems.

Recently, an increasing number of studies show evidence of the essential contribution of such large-scale convective systems to the global climatology. For example, in the paper of Liu and Zipser (2015), snapshots of precipitation systems (precipitation features (PFs)) observed by the precipi-

tation radar on board the Global Precipitation Mission (GPM) were analyzed. The largest PFs are found with sizes greater than 100,000 km^2. Liu and Zipser (2015) reported that PFs with size greater than 48,756 km^2 contribute 28% of total global precipitation. For PFs with size larger than 10,000 km^2, this contribution is 54%.

In the work of Khouider and Moncrieff (2015) a modified version of a previously developed multicloud model is used for parameterizing mesoscale convective systems (MCSs). For the condition of a typical double African and equatorial jet shear flow, a linear analysis of this modification shows an additional new scale-selective instability with a maximum of approximately 400 km. In addition, in the work of Kilpatrick and Xie (2015), surface wind observations from the Advanced SCATterometer (ASCAT) are utilized to estimate the downdrafts of MCSs. These observations show the existence of MCSs with the scale of 100-300 km.

On one hand, the GW spectra for MF1 and MF2 are not in agreement with the spectra observed by HIRDLS. On the other hand, there is an increasing number of recent studies showing the importance of large scale convective systems. This indicates a need of finding a new larger scale set for the CGWS scheme, which can correctly reproduce the spectrum observed by limb sounders. For this reason, we determine the free tunable parameters of the CGWS scheme ~~, which~~ that provide the best agreement with HIRDLS observations in this work. For that purpose a wide range of spatial and temporal scale sets of the CGWS scheme is surveyed. Based on that survey and observations from HIRDLS, combinations of scale sets which ~~fit best to~~ best fit the observed GW spectrum are selected for January and July 2006. Although simulations focus on the year 2006, similar convective regions are observed in different years (e.g. Ern et al., 2006; Alexander et al., 2008; Ern et al., 2011) and the current study aims to determine general characteristics of convective GWs by tuning the parameterization ~~grounded~~ based on observations. ~~For a further tuning of the simulated GW spectrum, the amplitude of individual waves is adjusted while keeping the same amount of total GWMF~~This will be supported by model-measurement comparison of three consecutive years. We also introduce an additional tuning parameter that controls the initial wave amplitude and therefore determines breaking levels. Details about this parameter will be explained later in the paper. For this purpose we compare zonal mean cross sections of observed and simulated GWMF and its vertical gradient. Again, the observational filter, which mimics the limitation of the instrument due to visibility effects and observation geometry, is applied to the simulations, and we can investigate the relation between absolute GWMF and GWD. Finally, we consider different source regions in global maps and discuss the interaction of GWs with the background wind employing phase speed spectra of the zonal momentum flux.

~~The paper~~ Till recently, several papers comparing single sources such as convection with observations have been published. Most of them are either completely theoretical using educated guesses for spectral distributions, or purely observational; some of them show correlations to proxies of deep convection (e.g. McLandress et al., 2000; Jiang et al., 2004; Jia et al., 2014). There are a few studies

which compare distributions in the hot spot regions (Choi et al., 2009, 2012). These studies used an educated guess to define the free parameters governing the spectral distribution and confine this guess by the global spatial distribution of GW variances. In our paper, for the first time, the spectral information by global observations is used to confine the spectral distribution in a CGW model. The spatial distributions are then used as an additional test. Furthermore, we estimate the relative importance of convective GWs for the momentum budget in different parts of the world. The step by step approach, confining the parameters first and using these for the global distributions again distinguishes this paper from previous studies.

The paper is organized as follows: In Sect. 2 we introduce the model setup. The systematic survey of different scale sets for the CGWS scheme is shown in Sect. 3. Also in Sect. 3 zonal mean cross sections of GWMF, its vertical gradient, GW drag as well as global maps and GWMF spectrum in terms of zonal phase speed and latitude are presented. Finally, summary and discussion are given in Sect. 4.

2 Model setup

Simulations are performed for January and July 2006 using three main elements: First, convective GWs are generated using the CGWS scheme developed at Yonsei University (Song and Chun, 2005). The waves are propagated upward using the Gravity wave Regional Or Global RAy Tracer (GROGRAT) (Marks and Eckermann, 1995; Eckermann and Marks, 1997). Finally, a comprehensive observational filter for limb sounders (Trinh et al., 2015) is applied for comparison with HIRDLS observations. These key components of our simulation are each briefly described in a subsection below.

2.1 Convective gravity wave source scheme

The Yonsei CGWS scheme is described in detail by Song and Chun (2005) and here only a short summary is given. This analytical model assumes a diabatic forcing region in a three-layer atmosphere. This three-layer atmosphere has a linear wind shear increasing from U_0 at the surface to U_t at an altitude lying between bottom height and top height of the diabatic forcing. Starting from that altitude level, the background wind is constant and equals U_t. Stability of this three-layer atmosphere is characterized by a piecewise function equaling N_1 below the cloud top and N_2 above the cloud top. Momentum flux due to gravity waves is calculated from the cloud top and can be presented as a function of horizontal phase speed:

$$\overline{M}(c) = -\operatorname{sgn}(U_t - c)\rho_0 \frac{2(2\pi)^2}{L_x L_t} \left(\frac{g}{c_p T_0 N_1^2}\right)^2 \frac{N_2}{|U_t - c|} |X|^2 \Theta(c) \quad (1)$$

Here c is the horizontal ground-based phase speed, ρ_0 is the air density at cloud top, L_x and L_t are appropriate spatial and temporal scales, respectively, used for averaging, c_p is the specific heat

of air at constant pressure, T_0 is the reference temperature at cloud top, $|X|^2$ represents resonance between vertical harmonics of natural wave modes and diabatic forcing. $|X|^2$ also represents gravity wave filtering by the ~~vertical propagation condition~~background wind during vertical propagation up to the cloud top. Therefore, $|X|^2$ is referred to as a wave-filtering and resonance factor. In the updated version of the CGWS scheme, Choi and Chun (2011) later redefined $\frac{N_2}{|U_t-c|}|X|^2$ as the wave-filtering and resonance factor. $\Theta(c)$ is the diabatic source function, which is ~~assumed to have a Gaussian-shaped in space and time~~described as follows:

$$\Theta(c) = \frac{2q_0^2}{\delta_x}\left(\frac{\delta_x\delta_t}{16\pi}\right)^2 \frac{\sqrt{\pi/2}}{\sqrt{1+(c-c_q)^2/c_0^2}} \tag{2}$$

where q_0 is the maximum magnitude of the diabatic forcing, c_q presents the moving speed of the forcing, and $c_0 = \delta_x/\delta_t$, where δ_x and δ_t are spatial and temporal scales of the forcing, respectively. The function $\theta(c)$ has a maximum at the phase speed equaling to c_q and monotonically decreases as $|c-c_q|$ increases (cf. Fig. 6a in Song and Chun, 2005).

The parameters q_0 and c_q as well as the cloud bottom and cloud top height needed to calculate the wave-filtering and resonance factor are determined from MERRA as follows: The vertical configuration of the heating is a 2nd order polynomial (cf. Eq. 8 of Song and Chun, 2005). Based on that assumption, heating profiles provided by MERRA data are fitted using a second order fit. Cloud top and cloud bottom data from the MERRA data set are used as a first guess for the second order fitting. Results of this second order fit are then used to recalculate top and bottom of the forcing regions. Also, the maximum value of the fitted heating profile between recalculated forcing top and forcing bottom is defined as q_0. The moving speed c_q is determined as the horizontal background wind averaged below 700mb (Choi and Chun, 2011).

The parameters δ_x and δ_t are free tunable parameters of this CGW source scheme. In this work we perform a systematic survey by running our simulations with different spatial and temporal scales. All the scales used for this survey are shown in the first two columns in Table 1. It should be noted that in previous studies the free input parameters δx and δt have been defined using educated guesses. In the current work, these parameters are defined using spectral information from observations. Therefore, we first keep an open mind and estimate δx and δt by adaption to the observed spectrum. A potential physical process related to these δx and δt values will be discussed later in the paper.

For computational efficiency the momentum flux spectrum $\overline{M}(c)$ is not sampled continuously, but up to 10 maxima in the phase speed range from -100 $\mathrm{m/s}$ to 100 $\mathrm{m/s}$ are selected. These discrete values are used as input for the GW ray tracer, launched at the cloud top, and propagated ~~way~~ away from the source. Shallow heating depths are not effective in exciting far-propagating GWs. Therefore, simulations are run only for heating depths equal or larger than 3.5 km. When coupling the GW ray tracer to the CGWS scheme, there is a further tuning potential to adapt the global distributions. We can reduce the launch amplitude by a factor of $1/\sqrt{\alpha}$ and simultaneously multiply the number of launched rays by a factor of α. In this way we retain the same total GWMF at launch

but reduce the amplitude of the individual waves. This may be interpreted by spreading the same total GWMF over a larger area, i.e. assuming that the wave packet has a ~~lager~~ larger spatial extent. An important consequence is that by reducing the amplitude of the individual waves, saturation is reached at higher altitudes in the atmosphere.

The ~~latent heat input data are~~ vertical profile of latent heat release is taken from three-hourly MERRA (modern-era retrospective analysis for research and applications) assimilated data~~.~~, which uses a parameterization for convection. The chief aim of the parameterization is to capture the total amount of rain and the vertical redistribution of water. That should confine the vertical structure of latent heat release. This is the only explicit input we require from MERRA for our study. Spatial and temporal scales of the convection are formulated in the CGWs scheme as described above. More detailed information about MERRA data as well as convective parameterization in MERRA can be found, for example, in Rienecker et al. (2011); Kim and Alexander (2013); Wright and Fueglistaler (2013).

2.2 The gravity wave ray tracer

In the current work, propagation of GWs from convective GW sources into the middle atmosphere is performed using GROGRAT. Details about this ray tracer are presented in (Marks and Eckermann, 1995; Eckermann and Marks, 1997). We here only give a brief description. GROGRAT is based on the full gravity wave dispersion relation, which includes both non-hydrostatic gravity waves and the Coriolis force. Wave packets are propagated according to the local group velocity of the wave depending on the wave vector and intrinsic frequency. The ray-tracing equations (Lighthill, 1967) are solved using a 4th order Runge Kutta integrator. The integration comprises the calculation of refraction of the wave vector caused by gradients of the atmospheric background in both vertical and horizontal directions. Wave action is calculated along the wave trajectory accounting for dissipation, damping, and saturation processes. Amplitude damping caused by turbulence is calculated following the work of Pitteway and Hines (1963). Radiative damping due to the temperature difference between warm and cold phases of the wave is considered following Zhu (1994). The saturated amplitude of the wave is limited using saturation criteria of Fritts and Rastogi (1985). Moreover, MERRA winds and temperature are used as atmospheric background for the ray-tracing calculations.

2.3 The comprehensive observational filter for satellite limb sounders

For comparing modeled results with HIRDLS observations, a comprehensive observational filter for satellite infrared limb sounding of gravity waves was applied. Details of this observational filter are described in Trinh et al. (2015). The observational filter considers both the visibility of waves to an infrared limb sounder and a sophisticated representation of the observation geometry. The absolute GWMF simulated by applying this observational filter to the model results can be directly compared

to the GWMF from observed temperature amplitudes (Ern et al., 2004):

$$F = \frac{1}{2}\rho\frac{\lambda_z}{\lambda_h}\left(\frac{g}{N}\right)^2\left(\frac{\hat{T}}{T}\right)^2 \quad (3)$$

where F denotes absolute GWMF, ρ is the background atmosphere density, λ_z and λ_h are vertical and horizontal wavelengths, respectively, g denotes the gravity acceleration, N is the buoyancy frequency, T is the background temperature and $\hat{T}$ is the temperature amplitude of the wave. Although Eq. 3 is based on monochromatic wave assumption while CGWs are a multiscale problem, it was shown that in a statistical sense, spectra of CGWs obtained from 2D Fourier transform can be well reproduced using a single-wave approach (Lehmann et al., 2012). Furthermore, our modeling approach is based on a number of discrete waves, which enhances compatibility between the two approaches. We thus expect, that no larger distortions of the spectrum are generated by the chosen approach.

The observational filter comprises four main processes: (1) visibility filter, (2) projection of the wavelength on the tangent-point track, (3) aliasing effect, and (4) calculation of the vertical observed wavelength. The first process (visibility filter) considers impacts caused by radiative transfer and retrieval (Preusse et al., 2002). This visibility filter directly influences the temperature amplitude $\hat{T}$. From HIRDLS observations information is provided only along measurement track. The horizontal wavelength along measurement track is generally larger than the real horizontal wavelength. The second process of the observational filter determines this along-track wavelength and the associated reduction of GWMF by modifying λ_h in Eq. 3. The aliasing effect (the third process) estimates the projection of waves towards much longer wavelengths by aliasing and the corresponding reduction of GWMF. Due to the aliasing effect, λ_h in Eq. 3 may have larger value and accordingly, F may decrease. The calculation of the vertical observed wavelength (the fourth process) addresses effects of non-vertical altitude profiles. Due to this effect, not only the vertical structure of an observed wave is sampled, but also to some extent the horizontal structure. The vertical wavelength λ_z in Eq. 3 therefore should be recalculated by considering this effect. Finally, additional corrections are applied that are required for the real satellite data to remove dominant vertical oscillation of quasi-stationary planetary waves as well as to keep only those vertical wavelengths for which amplitudes can reliably be determined in the 10 km vertical window of the MEM/HA spectral analysis (Preusse et al., 2002; Ern et al., 2011).

3 Results

3.1 A systematic survey of the Yonsei CGWS scheme

The purpose of this systematic survey is to find sets of free parameters δx and δt which describe spectra in terms of horizontal and vertical wave numbers observed by HIRDLS. For the systematic survey of the spatial and temporal scales we tested the whole set of combinations given by the

surveyed scales in the first two columns in Table 1. These scales are selected on one hand to cover the whole potential ranges, on the other hand with the appropriate step width to ~~optimize~~ minimize the number of different scales and therefore to improve the computational efficiency. An appropriate step width also helps to distinguish the changing of the spectrum in the base 10 logarithmic scale of the wave numbers.

Figure 1 provides an overview of the results ~~by~~ for a reduced set of filtered, simulated GW spectra. In Fig. 1, for a better visualization, only spectra corresponding to the values given in bold in Table 1 are shown. Spectra in Fig. 1 are shown for July 2006 at the altitude of 25 km and averaged over the same regions defined as deep convection (DC) regions in Ern and Preusse (2012). ~~These spectra~~ The location of these regions is indicated in Fig. 2; regions for boreal summer (Northern Hemisphere) are marked in red, regions for austral summer (Southern Hemisphere) are marked in green. The spectra in Fig. 1 are generated by binning absolute GWMF from ray-tracing ~~calculation~~ calculations according to horizontal and vertical wave numbers (k_h and m) using a technique similar to that of Ern and Preusse (2012). The base 10 logarithmic scale is employed here, i.e. the x axis shows $\widetilde{k_\mathrm{h}} = \log_{10}(1/\lambda_\mathrm{h})$ while the y axis shows $\widetilde{m} = \log_{10}(1/\lambda_z)$. Here λ_h and λ_z denote the horizontal and vertical wavelengths, respectively. The sizes of each bin in x and y direction are $\delta\widetilde{k_\mathrm{h}} = 0.1$ and $\delta\widetilde{m} = 0.1$.

In Fig. 1 the color shading represents the GWMF spectra simulated by the Yonsei CGWS, propagated to observation altitude by GROGRAT and filtered according to the comprehensive observational filter. The dashed contour lines indicate the spectrum observed by HIRDLS for regions of deep convection (Ern and Preusse, 2012). For the model spectra, spatial scale increases from the right column to the left column in Fig. 1. The temporal scale increases from the bottom to the top in Fig. 1. As shown by Fig. 1, the horizontal wavelength of the spectral peak increases as the spatial scale δx of the convective system increases. Due to the resonance effect formulated in the CGWS scheme, the phase speeds and hence the vertical wavelength of the spectral peak depends only weakly on the temporal scale δt of the convective system. We hence use the observed spectra to a) gain information on the horizontal scale, which is not determined by the model conception, but b) also to validate the vertical wavelength spectrum. This is a corroboration of the model assumptions. The comparison of the spectrum hence is a confirmation that the basic assumptions of the model describe reality well, at least in a statistical sense.

It can also be seen in Fig. 1 that GWs forced by convective systems with very short spatial and temporal scales (e.g. Fig. 1n, o, s, t) are strongly suppressed in HIRDLS observations due to the observational effect. Some of the spectra (e.g. Fig. 1g, h, l) show a spectral peak, which locates closely to the observed spectral peak. To complement the survey grid with a parameter set providing a close match with the observed spectral peak, we calculated additional spectra with $\delta x = 200$ km and $\delta t = 150$ min for January 2006 and $\delta x = 160$ km and $\delta t = 100$ min for July 2006.

As mentioned in the introduction, the large-scale convective system studies (Liu and Zipser, 2015; Khouider and Moncrieff, 2015; Kilpatrick and Xie, 2015) indicate that CGW forcing is a multi-scale problem with major contributions by a few dominant scales. For this reason we combine several spectra from the systematic survey in order to obtain a best fit to the observed spectra. Spectra are super-imposed by minimizing the following function:

$$\eta = M_{obs} - \sum_i \zeta_i M_i / \sum_i \zeta_i \tag{4}$$

where M_i is a single spectrum from the systematic survey, ζ_i is the respective intermittency factor, and M_{obs} is the observed GWMF spectrum. Combinations of M_i with respective ζ_i, which give the best fit to the observed spectrum, are chosen from minimization of η and shown in Fig. 3c for January and Fig. 3d for July 2006. For computational efficiency, we limit the maximum number of combined spectra to 4 and only largest ζ_i are selected. The selected spatial scale δx, temporal scale δt as well as corresponding intermittency factor ζ are shown in Table 1 for January and July 2006. As shown by Fig. 3c and Fig. 3d, the filtered simulated spectrum matches the observed spectrum very well in both shape and location of the spectral peak for both conditions of January and July 2006. The scales selected by our approach quantitatively agree well with those found in the convective system studies, which were mentioned in the introduction.

Moreover, it is noteworthy that ~~the GW spectrum is somewhat different for northern and southern hemisphere, and different~~ different combinations of scale sets are needed for January and July (cf. Table 1). ~~These scales quantitatively agree well with those found in the convective system studies, which were mentioned in the introduction. These scales determined by the regions of deep convection are then adopted for the convective sources in each hemisphere, respectively. By doing so, we assume that the observed GW spectra in these regions are dominated by CGWs. However, in other regions, other GW sources will be more dominant and direct comparison with the CGWS is less meaningful or even not possible. Therefore, adopting parameter choices determined by deep convection regions for the entire respective hemisphere is one of the limitations of our approach~~This leads to a question: Is the difference between January 2006 and July 2006 caused by a persistent difference between the two hemispheres or is it caused by the temporal variability of convective source processes? In order to investigate this question we have considered spectra for three consecutive years. This is described in the Appendix. In summary, we find a general tendency for longer horizontal wavelengths in the Southern Hemisphere caused by different source characteristics. We also find a modulation of the GW spectrum at 25 km altitude due to the QBO which can be reproduced with the same set of model parameters. This indicates that the QBO modulation is caused primarily by different propagation conditions of the GWs.

In addition, in order to demonstrate effects of the observational filter, we show unfiltered combined spectra of the same selected scale sets for January 2006 in Fig. 3a and for July 2006 in Fig. 3b. Comparison of Fig. 3a, b and Fig. 3c, d shows that the observational filter not only reduces the mag-

nitude, but also significantly changes the shape of the spectrum. In particular, contributions of short horizontal wavelength waves as well as short vertical wavelength waves strongly decrease and are also partly shifted to longer horizontal wavelengths. More details about effects of the observational filter on GW spectrum can be found in Trinh et al. (2015).

3.2 Zonal average of convective GWMF and its vertical gradients

In Sect. 3.1 the free parameters of the convective source scheme were estimated. In this section, ~~our calculations are based on the scale~~ we apply these parameters to global-scale simulations in order to estimate the effect of CGWs on the global distribution of GWMF and GW drag. There are limitations to our approach: The selected scales are determined in regions that are likely dominated by GWs that are excited by deep convection (see Fig. 2 for regions of deep convection). However, in regions which are not dominated by one source process, we cannot sort the observed waves according to sources, at least not based on current limb sounding observations. Comparison between observed and modeled spectra thus does not provide a meaningful constraint on the CGW source scheme parameters. Therefore the constraint from the regions of deep convection is the only observational guidance we have and which we consider preferential to a guess. Accordingly, in order to study the importance of CGWs on global scale, the selected sets of δx and δt ~~which were selected in Sect. 3.1.~~ are used globally for the convective sources for January and July, respectively.

Zonal averages of GWMF and its vertical gradient are calculated and shown in Fig. 4 for January and in Fig. 5 for July 2006. In all panels of Fig. 4 and Fig. 5, contour lines indicate zonal average zonal wind for the respective month. In order to generate zonal averages of absolute GWMF, the values from ray-tracing ~~calculation~~ calculations are first binned onto a three-dimensional grid with bin sizes of 10° in longitude, 2° in latitude and 1 km in altitude. Results are normalized by total number of rays and the zonal averages are calculated.

Figure 4a and Figure 5a show simulated absolute GWMF without observational filter effects for January and July, respectively. Unfiltered GWMF shown in Fig. 4a and Fig. 5a is calculated as: $F_{pb} = \sqrt{F_{px}^2 + F_{py}^2}$, where F_{px} and F_{py} are GWMF components in zonal and meridional direction, respectively, as determined from the ray-tracing calculations. Both Fig. 4a and Fig. 5a show a main maximum of GWMF in the summer subtropics spreading from the equator to about 25 ° S (Fig. 4a) or to about 25 ° N (Fig. 5a), which is consistent with the latitude band of deep convection (e.g. Jiang et al., 2004). The width and magnitude of this maximum decreases with altitude due to wave dissipation, wave breaking and wind filtering. For January, this decrease is significant and strongly related to wind filtering at the altitude of about 20 km, where GWs encounter a wind reversal.

Figure 4b and Figure 5b show filtered, simulated absolute GWMF for January and July, respectively. Due to the observational filter the magnitude of GWMF is reduced by about half an order of magnitude. ~~Moreover, for January, stronger GWMF reduction is found at altitudes below and around the tropopause.~~

Observed GWMF from HIRDLS for January and July are shown in Fig. 4c and Fig. 5c, respectively. It should be noted that observations from HIRDLS shown in Fig. 4 and Fig. 5 contain global data of all regions, not only the regions of deep convection. For comparing filtered, simulated GWMF (Fig. 4b, Fig. 5b) with observed GWMF (Fig. 4c, Fig. 5c) it is very important to keep in mind that the model results show GWMF only from convective sources, while observations from HIRDLS contain GWMF from a variety of sources. As convection is believed to dominate the summer subtropics, we expect model and observations to better match at low latitudes~~while at~~. At mid and high latitudes HIRDLS observations indicate an ~~additional enhancement~~enhancement, likely due to other sources. Considering these facts, the simulated maximum in Fig. 4b and the secondary maximum in Fig. 4c in the summer subtropics match well. The same agreement can be seen by comparing Fig. 5b and Fig. 5c. In particular, centers of these maxima are both located at about 15 ° S for austral summer (Fig. 4b, c) or at about 15 ° N for boreal summer (Fig. 5b, c). Also, the structure of these maxima in the tropics from about 20 km to about 40 km altitude in both simulations and observations follow the contour line of the wind reversal. However, the magnitude of the simulated maximum is somewhat lower than the observed one. Moreover, the width of the simulated maximum is slightly narrower than the observed one. ~~These differences can be interpreted by a lack of contributions from other sources than convection~~The weaker and narrower peak in the simulations could indicate that deep convection is spread over a wider latitude range than simulated in MERRA or that we need to revisit the forcing efficiency. However, there is also indication from radiosonde and ground-based measurements (e.g. Leena et al., 2010; Pramitha et al., 2015) and modeling (e.g. Preusse et al., 2014) indicating that related to regions of deep convection GWs are excited around the tropopause. Details of that GW excitation are not fully understood, but they are presumably associated with the shear and strong buoyancy change present at these altitudes. These waves seem to be less focused to the convective regions and produce a substantial background outside the selected convection regions used for the spectra (cf. Fig. 4c and Fig. 5c) and thus potentially become important in the zonal means. At high winter latitudes, CGWs contribute only a minor part of the total GWMF. This can be seen from the unfiltered GWMF values as well.

Different measures of the vertical gradient:

Vertical cross sections of the absolute value of GWMF span several orders of magnitude and accordingly a logarithmic color scale is used, which emphasizes the major features while the precise vertical structure is difficult to discern. On the other hand, for discussing the interaction of GWs with the background flow it is important to consider the exerted zonal mean drag in the zonal direction~~:~~. We calculate the drag by calculating the vertical change of zonal momentum flux along the ray. In this way the calculations take into account wave dissipation and horizontal refraction but do not cause a spurious acceleration where GWs just propagate horizontally out of a region where we

calculate the vertical gradient. The zonal mean drag in the zonal direction is calculated as follows:

$$X = -\langle 1/\rho \cdot d/dz(\frac{\partial}{\partial z} F_x) \rangle \tag{5}$$

where ρ is atmospheric density, F_x is the zonal GWMF and $\langle\,\rangle$ denotes the zonal mean. Unfortunately measurements can provide only vertical gradient P:

$$P = -\langle 1/\rho \cdot d/dz(\frac{\partial}{\partial z} |\Omega(\boldsymbol{F})|) \rangle \tag{6}$$

where $\boldsymbol{F}$ is the horizontal vector of GWMF, Ω denotes the observational filter and $|\,|$ denotes absolute values in 2D, i.e. here $\sqrt{\Omega(F_x)^2 + \Omega(F_y)^2}$, where F_y is the meridional GWMF. In fact, differences between X and P can be significant: waves dissipating, because they reached saturation amplitudes, but propagating in opposite directions cancel each other when calculating X but contribute both positively in calculating P. Moreover, waves propagating conservatively but moving out of the observational filter Ω will enhance P but they do not contribute to the real drag X. Therefore, P may exhibit different patterns from X. However, P still emphasizes the vertical gradient and in this respect it is the closest proxy for X we can gain from measurements. The model setup of this paper allows us to calculate both X and P and hence to compare P to the observations. Furthermore, we can study the various contributions of dissipation, drag and observational filter by calculating different combinations of the vertical derivative, the observational filter and the absolute value.

Physical interpretation:

Figure 4d and Figure 5d show the simulated zonal drag X for January and July 2006, respectively. In the tropics (15 ° S-15 ° N), in the lower and mid stratosphere (i.e. up to about 35 km) drag is exerted in regions of vertical wind shear. ~~Positive drag is found~~ There we find positive drag for positive shear and negative drag for negative shear as expected for the driving of the QBO. Moreover, the magnitude of the simulated zonal drag X is comparable to the "missing drag" deduced in Ern et al. (2014). In Ern et al. (2014), in order to estimate the QBO driving by GWs, the transformed Eulerian mean zonal momentum equation (Andrews et al., 1987) was utilized. All terms of this equation except the drag due to GWs were calculated using ERA-Interim assimilated data (Dee et al., 2011). The drag due to GWs is then deduced based on this equation and other calculated terms and is referred to as the "missing drag". In addition, for January 2006, Fig. 4d shows a particularly noteworthy U-shaped structure around 30 km.

The closest similarity to observed potential drag is provided by P, which takes into account reduction of observed GWMF both by dissipation and by the fact that waves are moving out of the observational filter. In order to distinguish between these two processes we introduce a further quantity which shows only the true dissipation we observe. Figure 4e and Figure 5e show another type of vertical gradient of GWMF, which is calculated as follows:

$$Q = -\langle 1/\rho \cdot |\Omega(d/dz(\frac{\partial}{\partial z} \boldsymbol{F}))| \rangle \tag{7}$$

The vertical gradient Q only considers the dissipation caused by those waves ~~only~~ which are visible to the instrument. This also means that dissipation of waves which are not seen by the instrument is not taken into account in Q even though these waves exert real drag and are taken into account in calculating X. In Fig. 4e the U-shaped structure is much less pronounced in comparison with Fig. 4d, ~~but~~ which indicates that the drag is exerted when the waves attained very short vertical wavelength and are already removed by the observational filter from Q. Such short vertical wavelengths would also mean that critical level filtering is an important process in this region.

In both Fig. 4e and Fig. 4d, strong dissipation can be seen for a wind maximum at 40-45 km altitude and 20 ° S, which is located above the strongest sources~~and associated rather to a wind maximum than to a vertical gradient of~~ . The maximum is similar strong in Q and in P indicating that observational filter effects are less important. This is the case for waves with vertical wavelengths longer than the short-wavelength edge of the observational filter. This also means that critical level filtering is not relevant at this point. For longer vertical wavelengths, dissipation may be reached just by the exponential amplitude growth which compensates the decrease of atmospheric density. This is particularly likely in regions where GW amplitudes are large already at excitation level. The net drag in Fig. 4d is low indicating that waves from both propagation directions contribute, which is compatible with saturation by amplitude growth. A small preferential net drag in this case is caused by a preferential direction in GWMF. Similar strong dissipation can be seen at the same altitude range at about 20 ° N in Fig. 5~~e.~~ d and Fig. 5e. Here the preference in propagation direction and net drag are considerably stronger. This dissipation in the upper stratosphere is important for the driving of the SAO in the tropics (cf. discussion in Ern et al., 2015).

Figure 4f and Figure 5f show simulated P (the quantity observations should be compared to). For January, both the U-shaped structure at around 30 km and the maximum above 40 km are visible and correspond well to similar structures in the observed vertical gradient from HIRDLS (Fig. 4g). In Fig. 4d and Fig. 4f, the U-shaped structure is more pronounced than in Fig. 4e. A possible reason for this difference is: In the U-shaped structure we presumably see many waves of low horizontal phase speeds which are refracted to very short vertical wavelengths and therefore are not visible to the satellite instrument. As the saturation is reached only when the vertical wavelength is even shorter than the short edge of the visibility filter, these waves propagating from below first do not pass the observational filter any longer (absence in Fig. 4f at 30 km altitude and 15 ° N) but dissipate almost immediately above (Fig. 4d at 30-33 km and 15 ° N). The dissipation itself is then not visible to the satellite (low values of vertical gradient at 30-33 km and 15 ° N in Fig. 4e). It should be mentioned that a related shift in the altitude of observed GWD has been discussed in Ern et al. (2014).

As we mentioned in Sect. 2.1, ~~there is a further tuning potential~~ further tuning is achieved by reducing the launch amplitude by a factor of $1/\sqrt{\alpha}$ and simultaneously ~~multiply~~ multiplying the number of launched rays by a factor of α. In this ~~work,~~ study α is chosen to be 5. The choice of α does not affect the total GWMF at launch but can affect GWMF ~~at higher altitudes and shift~~ aloft,

shifting the saturation level to ~~higher~~ different altitudes. Therefore, depending on the choice of α structure and magnitude of GWMF, zonal drag, simulated P, and simulated Q may be altered. With a more detailed consideration of the momentum balance this tuning factor may need to be revisited.

The GW drag maximum at 40 to 45 km altitude is seen in Fig. 4e, 4f and 4g, but not in Fig. 4d. This is likely caused by longer vertical wavelength waves having gained saturation amplitude but not causing much net GW drag as different propagation directions contribute. In July we find closer correspondence between P and X (again with some altitude shift). The structures of P and X also agree quite well with the structures of observed vertical gradient shown in Fig. 5g. Similar to GWMF, the observed vertical gradients in Fig. 4g and Fig. 5g are dominated, in particular at higher latitudes, by signatures from sources other than convection. It should also be noted that a 10 km vertical analysis interval is used for HIRDLS data analysis, which could also lead to some differences between model results and observations.

3.3 Horizontal distribution of GWMF and phase speed spectrum

In this section we show horizontal distributions of simulated convective GWMF as well as spectra of GWMF in terms of zonal phase speed and latitude. In Fig. 6 and Fig. 7 data for January, and in Fig. 8 and Fig. 9 data for July are shown. Figures 6 and 8 give values for 25 km altitude, while Fig. 7 and 9 give values for 40 km altitude. In each of these figures, the left column contains global maps of GWMF: panel (a) the unfiltered, simulated GWMF, panel (c) the filtered, simulated GWMF and panel (e) the observed GWMF. The right column shows zonal GWMF as a function of zonal phase speed and latitude (hereafter referred to as phase speed spectra) in bins of 4 $\mathrm{m/s}$ and 4 $^\circ$. For both maps and spectra the color scales indicate the base 10 logarithm of GWMF. As for phase speed spectra GWMF with negative (westward) phase velocities is negative (westward GWMF), these values were multiplied by -1 before applying the logarithm. HIRDLS does not provide a propagation direction and accordingly phase speed cannot be deduced from the measurements.

In the global maps (panels (a), (c), (e)), the rectangle indicated by the magenta dashed line shows the low latitude area, where convection is assumed to dominate. Blank areas in panels (a), (c), (e) refer to values of GWMF, which are out of the shown value range (< -5.0 $(\log_{10}\mathrm{Pa})$ or > -1.0 $(\log_{10}\mathrm{Pa})$). In panels (b), (d), the gray thick line indicates zonal mean of zonal wind at the considered altitude level, magenta plus line shows maximal zonal mean of zonal wind in the altitude range from cloud top to the considered altitude level, and magenta dot line shows minimal zonal mean of zonal wind in the same altitude range.

For January 2006, at 25 km altitude, high values of unfiltered GMWF are found over central south America, south Africa, a strip spreading from Madagascar to Indonesia, Indonesia and north Australia, and a strip over the Pacific ocean at around 20° S latitude spreading from 180° W to 120° W (Fig. 6a). After applying the observational filter, GWMF decreases about half an order of magnitude (Fig. 6c). In addition, the observational filter also changes the distribution of GWMF at some loca-

tions. For example, over Indonesia region, a band of high GWMF at about 10° N spreading from the Philippines to 180° E, is stronger filtered out in comparison with the band of high GWMF at about 0-10° S. Figure 6e shows observed GWMF from HIRDLS. Comparison of filtered GWMF (Fig. 6c) and observed GWMF (Fig. 6e) shows a quite good agreement in location of GWMF peaks in the summer subtropics. In particular, the maxima over central south America, south Africa, Indonesia and north Australia are reproduced. The magnitude of filtered GWMF is lower in comparison with observed GWMF which, as discussed above, can be explained by a lack of other sources than convection.

The phase speed spectrum for January 2006 at 25 km altitude (Fig. 6b) shows a major peak in the tropics with eastward phase speed from several $\mathrm{m/s}$ to about 25 $\mathrm{m/s}$, with the center of the peak at about 5 $\mathrm{m/s}$. At higher phase speeds (beyond 40-50 $\mathrm{m/s}$), two minor peaks in both eastward and westward directions are found. The GWMF associated with these minor peaks is about 2 orders of magnitude lower in comparison with the main peak. In mid and high latitude regions, high GWMF values are mainly associated with westward phase speeds varying from several $\mathrm{m/s}$ to about 40 $\mathrm{m/s}$. Figure 6d shows the phase speed spectrum of filtered GWMF. The observational filter in this case reduces GWMF magnitude but almost does not impact the spectrum structure.

The effect of wind filtering can also be found in the phase speed spectrum. This effect occurs when a wave encounters the critical level, i.e. where the background wind equals the phase speed of the wave. In this case, the intrinsic phase speed and thus the vertical wavelength approach zero causing saturation and the release of GWMF. In Fig. 6b and 6d, GWMF are mainly found in the areas where GW phase speed is larger than maximal zonal mean of zonal wind (magenta plus line) or lower than minimal zonal mean of zonal wind (magenta dotted line). A small amount of GWMF still can be found in between these two lines because: a) these lines only indicate the zonal mean of the zonal wind and thus waves may be able to propagate due to local variations and b) many waves also have a meridional component. Still the findings indicate that filtering is dominated by the variation of the zonal wind.

For January 2006 at 40 km altitude, the horizontal band of high GWMF values in the summer subtropics becomes narrower (more concentrated around latitude of $\sim$15°S) and is slightly shifted poleward. The magnitude of GWMF decreases strongly with altitude, as can be seen by comparing Fig. 6a and Fig. 7a. This is also in agreement with the vertical cross section of absolute GWMF shown in Fig. 4a. A wind reversal at about 30 km altitude is likely the main reason for the reduced GWMF values close to the equator, or in other words, for narrowing the horizontal band of high GWMF values. The location of simulated and observed GWMF hot spots agrees well (cf. Fig. 7a, b, c). At 40 km altitude the measurements indicate that GWMF in the hot-spot regions, where the model results suggest deep convection as the dominant source, is enhanced about one order of magnitude compared to the background regions. This is a stronger enhancement than at 25 km altitude

(about half an order of magnitude) and indicates that the non-convective background is relatively less important at 40 km.

Also the phase speed spectrum changes with altitude: the main peak of the spectrum at 40 km does not stretch over the equator as for 25 km but is limited only to the southern hemisphere. This change is according to the change of the maximal zonal wind, which is indicated by the magenta plus line. This line surrounds the main peak in the tropics. Another major difference of the phase speed spectrum at 40 km in comparison with the one at 25 km is the absence of the peak at mid and high latitudes in the southern hemisphere at westward phase speeds (20°S to 40°S). This absence is again likely related to wind filtering as indicated by the magenta dotted lines for the difference in minimum zonal winds in Fig. 6b, d and Fig. 7b, d, respectively.

For July 2006 at 25 km altitude, unfiltered GWMF (Fig. 8a) shows high values over the Caribbean sea, central Africa and the Asian Monsoon region. Figure 8c shows filtered GWMF with the magnitude reduced significantly due to the observational filter. Comparison of filtered GWMF (Fig. 8c) and observed GWMF (Fig. 8e) shows a quite good agreement in locations of GMWF maxima. As seen before in the zonal means, however, the observed GWMF maxima are wider, i.e. extend further to the north. In addition, the model results also show GW excitation following the warm water currents of the Gulf Stream and the Kuroshio.

Similar to January 2006 at 25 km altitude, the phase speed spectra (Fig.8b and Fig. 8d) show a main peak in the summer subtropics with eastward phase speeds from several $\mathrm{m/s}$ to $\sim$30 $\mathrm{m/s}$. Moreover, two secondary peaks in the summer subtropics at high phase speeds (larger than 40-50 $\mathrm{m/s}$), which are $\sim$2.5 order of magnitude smaller in comparison with the main peak, are also found. The observational filter decreases the GWMF magnitude but almost does not alter the structure of the phase speed spectrum. This can be seen by comparing the spectrum structure shown Fig.8b and Fig. 8d.

Similar to the January case, the magnitude of GWMF decreases with altitude (Fig. 9). This decrease, however, is weaker than in January. In particular, there is no strong reduction of GWMF in the tropics, which narrows the region of strong GWMF between 25 km and 40 km, such as for January.

Concerning the phase speed spectrum at 40 km altitude (Fig. 9b, d), a major difference in comparison with the spectrum at 25 km is much lower GWMF at mid and high latitudes in the northern hemisphere (from 40°N - 80°N). This can be seen by comparing Fig. 8b, d with Fig. 9b, d. This reduction is likely related to the change of minimal zonal wind at this latitude range, which can be seen by comparing minimum zonal mean of zonal wind in Fig. 8b, d and Fig. 9b, d, respectively.

4 Summary and discussion

In this study, ~~spatial and~~ the free parameters δx and δt representing the horizontal and temporal scales of the ~~CGWS scheme (Song and Chun, 2005) are systematically tuned to find the best match between simulated and observed horizontal and vertical wave number spectra of GWMF~~convection are derived; the strength and vertical structure of the heating are calculated from MERRA analysis data. The trajectory calculation for convective GWs generated by the CGWS scheme is performed using GROGRAT (Marks and Eckermann, 1995; Eckermann and Marks, 1997). For comparison with HIRDLS observations, a comprehensive observational filter (Trinh et al., 2015) is applied. The observed spectra can be well reproduced in terms of spectral shape and location of the peak by super-imposing four scale sets. The spectral shape of GWMF in the summer subtropics is different for January and July. Matching of simulated and observed spectra can only be achieved by different combinations of scale sets of the convective source indicating that this is an effect of the source properties rather than of the propagation conditions or observational filter. We considered three different years and found that in the Southern Hemisphere, source characteristics of the GWs cause consistently longer horizontal wavelengths. We also found a modulation of the spectrum due to a modulation of the propagation conditions by the QBO. This modulation of the spectrum can be reproduced using the same set of CGW source parameters during different years.

We used the parameters determined from the spectra and considered the contribution of these waves to the momentum balance by calculating zonal mean cross sections of absolute GWMF and its vertical gradients and compared them to respective observed quantities. The approach is limited by the fact that we have to use globally the CGW scheme parameters estimated for the subtropics, which is the only observational constraint available. The zonal average of filtered simulated GWMF is consistent with observed GWMF in the summer subtropics in both structure as well as magnitude. Applying the observational filter to the model, we find that in the mid stratosphere in regions of wind shear, slow GWs are refracted to very short vertical wavelength. Consequentially, these waves cannot pass our observational filter and remain invisible whilst dissipating and exerting GWD at the location closely above the altitude where they become invisible to the instrument. Close to the stratopause waves of longer vertical wavelengths from all propagation directions reach saturation amplitudes and dissipate, in some cases without exerting much net drag. Similar to the absolute GWMF, the vertical gradient of filtered GWMF agrees well with the observed vertical gradient. Values of simulated zonal drag X are of the same order as the expected GW driving of the QBO (Ern et al., 2014). This indicates that GWs from convection organized at scales of the order of 100 km are important for driving the QBO.

Horizontal distributions of absolute unfiltered and filtered GWMF are also presented in this work. These horizontal distributions show a good agreement with observed horizontal distributions in the structure as well as the magnitude. Main convection hot spots are well reproduced. We also showed the GWMF spectra in terms of zonal phase speed and latitude. These spectra show a main peak in

the tropics and summer subtropics associated with eastward phase speeds between several $\mathrm{m/s}$ and about 30 $\mathrm{m/s}$. As CGWs are commonly believed to dominate the tropics and subtropics, these phase speed spectra are expected to match respective observations of the same regions.

The vertical gradient of absolute GWMF provided by measurements is not always an indication of drag. At places where GWs have grown to reach saturation amplitudes contributions from different propagation directions cancel each other. We see such a case, for instance, in the southern subtropics around the stratopause in January. In addition, waves may leave the observational filter but do not break. For instance, it was argued by Alexander (2015) that in this way the comparison of vertical gradients of observed absolute GWMF with a momentum balance of the QBO shown by Ern et al. (2014) is not meaningful. The spectra inferred in this study show that zonal wind filtering of GWMF occurs for slow phase speed waves and in a very similar way for unfiltered and filtered simulations. Accordingly, in the zonal means there is a large similarity between simulated P (the quantity corresponding to observations) and the absolute values of simulated drag Q. The only effect we can find is that waves first leave the observational filter and break soon after above, which shifts the observed "drag" downward in comparison to the real drag, an effect which was already discussed by Ern et al. (2014). Regarding wave saturation effects, it has been discussed by Ern et al. (2015) that the situation becomes more complicated if wave saturation apart from critical levels occurs. In this case, additional information about the GW spectrum may be required (for example, like pre-filtering of the GW spectrum by the winds at lower altitudes) to correctly interpret vertical gradients of observed absolute GWMF.

Due to the limitations of current global observations, the synergetic use of physics-based models, observational filter and observations using both absolute values of GWMF and its vertical gradient is currently the most promising way to infer the true properties of GWs in the atmosphere. GWs from single convective cells with horizontal scales of a few kilometers cannot be constrained by limb sounder data and exist in parallel as studies using different instruments show (Choi et al., 2009, 2012). The GWs exited by such events are clearly subgrid to global models and need to be parameterized, but also larger scale CGWs from organized convection may not well be represented depending on the convection parameterization (Ricciardulli and Garcia, 2000; Kim et al., 2007; Preusse et al., 2014) and would in this case need to be parameterized, even if the scales of potentially resulting GWs could be resolved by the dynamical core of the model.

Appendix A: Interannual variability and consistent differences between Southern and Northern Hemisphere

In this section, we address how the interannual variation of spectra compares to the difference between the spectra for the two hemispheres. Spectra are calculated for the deep convection regions defined by Ern and Preusse (2012) and shown in Fig. 2. For boreal summer (June, July, August) spectra are calculated for the regions marked in red, for austral summer (December, January, Febuary) spectra are calculated for the regions marked in green. In Fig. A1, panels (a) (b) (c) show spectra averaged for boreal summer for 2005, 2006, 2007 respectively; panels (d), (e), (f) show spectra averaged for austral summer for 2005/6, 2006/7, 2007/8. Therefore, each row in Fig. A1 can be considered as the spectra of the different hemispheres of the same year.

From Fig. A1, it can be seen that regarding the magnitude of momentum fluxes, there is considerable year-to-year variability in the Northern Hemisphere and weaker variability in the Southern Hemisphere. Time series of GW momentum flux from SABER (Ern et al., 2011) indicate that these variations are related to the QBO. Considering all three rows, there is a consistent difference in the overall shape of the spectral distributions for the Northern and Southern Hemisphere, respectively. In addition, for one hemisphere, the peak vertical wavelength is slightly longer in years of stronger momentum flux. On the other hand, for a given hemisphere, the peak horizontal wavelength is very similar for different years.

In order to show the variation of the horizontal wavelength more clearly, we produced line plots of the horizontal spectral distribution. Normalized GWMF spectra at a vertical wavelength of 9 km are shown in Fig. A2. The value of 9 km is chosen because for all spectra 9 km is close to the peak value. In Fig. A2, the solid lines show the spectra for Northern Hemisphere and the dashed lines show spectra for Southern Hemisphere. In particular, solid blue, green, and red lines show spectra averaged for boreal summer (June-August) for 2005, 2006, 2007 respectively. Dashed blue, green, and red lines show spectra averaged for austral summer (December-February) for 2005/6, 2006/7, 2007/8. The differences among solid lines or among dashed lines are smaller than the difference between these two groups. The spectra for the Southern Hemisphere (dashed lines) are persistently peaking at lower horizontal wavenumbers (longer horizontal wavelengths) compared to the Northern Hemisphere spectra.

We now apply the scale sets that we found based on observations of 2006 to simulate spectra of the different hemispheres for different years. The simulated spectra at 25 km altitude are shown in Fig. A3. In Fig. A3, the color code shows the simulated GWMF spectrum and the dashed contour lines show the respective observed spectrum. As Fig. A3 shows, the scale sets selection based on observations of 2006 can reproduce the observed spectra of the same hemisphere for other years quite well. It is noteworthy that the year-to-year variability is well captured by these simulations (cf. Fig. A3 and Fig. A1). This year-to-year variation is particularly visible in the Northern Hemisphere, presumably associated with the QBO. An exception is the Southern Hemisphere in 2007 which

exaggerates the interannual variations in the simulation (cf. Figure A3 e). The disagreement for the Southern Hemisphere, 2007 therefore will be subject for further investigation.

The year-to-year variability, in particular for the Northern Hemisphere, is reproduced using only one set of GW source parameters for all years. This indicates that the variability is introduced by the QBO via the variation of propagation conditions and not by a variation of the source characteristic. In particular, this is consistent with the fact that the vertical wavelength changes between different years but not the horizontal wavelength.

In addition, we tested whether simulations based on the Southern Hemisphere setup of selected scales can reproduce observed Northern Hemisphere spectra, i.e., the setup of the opposite (wrong) hemisphere is used for this simulation. As an example, this simulation was carried out for July 2006. The results are shown in Fig. A4. The simulations comprise effects of the observational filter and modulation by the background wind. The fact that using the setup of Southern Hemisphere cannot reproduce the observed spectrum of the Northern Hemisphere is therefore an indication that the difference in the observed spectra is not caused merely by observational filter effects, i.e. that there is a real difference in the GW source characteristics (scales) for the two hemispheres.

Acknowledgements. MERRA data were provided by NASA and are available at http://disc.sci.gsfc.nasa.gov/mdisc/. HIRDLS data were provided by NASA and are available at http://disc.sci.gsfc.nasa.gov/Aura/data-holdings/HIRDLS/. This work was funded in part by the Deutsche Forschungsgemeinschaft (DFG) via the project MS-GWaves/SV (PR 919/4-1). H.-Y. Chun and M.-J. Kang were supported by the Korea Meteorological Administration (KMA) Research and Development Program under Grant KMIPA 2015-6160.

References

Alexander, M. J.: Global and seasonal variations in three-dimensional gravity wave momentum flux from satellite limb-sounding temperatures, Geophys. Res. Lett., 42, 6860–6867, doi:10.1002/2015GL065234, 2015.

Alexander, M. J. and Ortland, D. A.: Equatorial waves in High Resolution Dynamics Limb Sounder (HIRDLS) data, J. Geophys. Res., 115, D24111, doi:10.1029/2010JD014782, 2010.

Alexander, M. J. and Rosenlof, K. H.: Gravity-wave forcing in the stratosphere: Observational constraints from the Upper Atmosphere Research Satellite and implications for parameterization in global models, J. Geophys. Res., 108, doi:10.1029/2003JD003373, 2003.

Alexander, M. J., Gille, J., Cavanaugh, C., Coffey, M., Craig, C., Dean, V., Eden, T., Francis, G., Halvorson, C., Hannigan, J., Khosravi, R., Kinnison, D., Lee, H., Massie, S., and Nardi, B.: Global estimates of gravity wave momentum flux from High Resolution Dynamics Limb Sounder (HIRDLS) observations, J. Geophys. Res., 113, doi:10.1029/2007JD008807, 2008.

Alexander, M. J., Geller, M., McLandress, C., Polavarapu, S., Preusse, P., Sassi, F., Sato, K., Eckermann, S. D., Ern, M., Hertzog, A., Kawatani, Y., Pulido, M., Shaw, T., Sigmond, M., Vincent, R., and Watanabe, S.: Recent developments in gravity wave effects in climate models, and the global distribution of gravity wave momentum flux from observations and models, Q. J. Roy. Meteorol. Soc., 136, 1103–1124, doi:10.1002/qj.637, 2010.

Andrews, D. G., Holton, J. R., and Leovy, C. B.: Middle Atmosphere Dynamics, vol. 40 of *International Geophysics Series*, Academic Press, 1987.

Beres, J. H., Alexander, M. J., and Holton, J. R.: A method of specifying the gravity wave spectrum above convection based on latent heating properties and background wind, J. Atmos. Sci., 61, 324–337, 2004.

Choi, H. J. and Chun, H. Y.: Momentum flux spectrum of convective gravity waves. Part I: An update of a parameterization using mesoscale simulation, J. Atmos. Sci, 68, 739–759, doi:10.1175/2010JAS3552.1, 2011.

Choi, H.-J., Chun, H.-Y., and Song, I.-S.: Gravity wave temperature variance calculated using the ray-based spectral parameterization of convective gravity waves and its comparison with Microwave Limb Sounder observations, J. Geophys. Res., 114, D08111, doi:10.1029/2008JD011330, 2009.

Choi, H.-J., Chun, H.-Y., Gong, J., and Wu, D. L.: Comparison of gravity wave temperature variances from ray-based spectral parameterization of convective gravity wave drag with AIRS observations, J. Geophys. Res., 117, D05115, doi:10.1029/2011JD016900, 2012.

Chun, H.-Y. and Baik, J.-J.: Momentum Flux by Thermally Induced Internal gravity Waves and Its Approximation for Large-Scale Models, J. Atmos. Sci., 55, 3299–3310, 1998.

Chun, H.-Y. and Baik, J.-J.: An Updated Parameterization of Convectively Forced Gravity Wave Drag for Use in Large-Scale Models, J. Atmos. Sci., 59, 1006–1017, 2002.

Dee, D. P., Uppala, S. M., Simmons, A. J., Berrisford, P., Poli, P., Kobayashi, S., Andrae, U., Balmaseda, M. A., Balsamo, G., Bauer, P., Bechtold, P., Beljaars, A. C. M., van de Berg, L., Bidlot, J., Bormann, N., Delsol, C., Dragani, R., Fuentes, M., Geer, A. J., Haimberger, L., Healy, S. B., Hersbach, H., Holm, E. V., Isaksen, L., Kallberg, P., Koehler, M., Matricardi, M., McNally, A. P., Monge-Sanz, B. M., Morcrette, J. J., Park, B. K., Peubey, C., de Rosnay, P., Tavolato, C., Thepaut, J. N., and Vitart, F.: The ERA-Interim reanaly-

sis: configuration and performance of the data assimilation system, Q. J. R. Meteorol. Soc., 137, 553–597, doi:10.1002/qj.828, 2011.

Dunkerton, T. J.: The role of gravity waves in the quasi-biennial oscillation, J. Geophys. Res., 102, 26 053–26 076, 1997.

Eckermann, S. D. and Marks, C. J.: GROGRAT: a New Model of the Global propagation and Dissipation of Atmospheric Gravity Waves, Adv. Space Res., 20, 1253–1256, 1997.

Ern, M. and Preusse, P.: Quantification of the contribution of equatorial Kelvin waves to the QBO wind reversal in the stratosphere, Geophys. Res. Lett., 36, L21801, doi:10.1029/2009GL040493, 2009.

Ern, M. and Preusse, P.: Gravity wave momentum flux spectra observed from satellite in the summertime subtropics: Implications for global modeling, Geophys. Res. Lett., 39, L15810, doi:10.1029/2012GL052659, 2012.

Ern, M., Preusse, P., Alexander, M. J., and Warner, C. D.: Absolute values of gravity wave momentum flux derived from satellite data, J. Geophys. Res., 109, doi:10.1029/2004JD004752, 2004.

Ern, M., Preusse, P., and Warner, C. D.: Some experimental constraints for spectral parameters used in the Warner and McIntyre gravity wave parameterization scheme, Atmos. Chem. Phys., 6, 4361–4381, 2006.

Ern, M., Preusse, P., Gille, J. C., Hepplewhite, C. L., Mlynczak, M. G., Russell III, J. M., and Riese, M.: Implications for atmospheric dynamics derived from global observations of gravity wave momentum flux in stratosphere and mesosphere, J. Geophys. Res., 116, D19107, doi:10.1029/2011JD015821, 2011.

Ern, M., Preusse, P., Kalisch, S., Kaufmann, M., and Riese, M.: Role of gravity waves in the forcing of quasi two-day waves in the mesosphere: An observational study, J. Geophys. Res. Atmos., 118, 3467–3485, doi:10.1029/2012JD018208, 2013.

Ern, M., Ploeger, F., Preusse, P., Gille, J. C., Gray, L. J., Kalisch, S., Mlynczak, M. G., Russell, J. M., and Riese, M.: Interaction of gravity waves with the QBO: A satellite perspective, J. Geophys. Res. Atmos., 119, 2329–2355, doi:10.1002/2013JD020731, http://dx.doi.org/10.1002/2013JD020731, 2014.

Ern, M., Preusse, P., and Riese, M.: Driving of the SAO by gravity waves as observed from satellite, Ann. Geophys., 33, 483–504, doi:10.5194/angeo-33-483-2015, 2015.

Evan, S., Alexander, M. J., and Dudhia, J.: WRF simulations of convectively generated gravity waves in opposite QBO phases, J. Geophys. Res., 117, D12117, doi:10.1029/2011JD017302, 2012.

Fritts, D. and Alexander, M.: Gravity wave dynamics and effects in the middle atmosphere, Rev. Geophys., 41, doi:10.1029/2001RG000106, 2003.

Fritts, D. C. and Rastogi, P. K.: Convective and dynamical instabilities due to gravity wave motions in the lower and middle atmosphere: theory and observations, Radio Sci., 20, 1247–1277, 1985.

Jia, J. Y., Preusse, P., Ern, M., Chun, H.-Y., Gille, J. C., Eckermann, S. D., and Riese, M.: Sea surface temperature as a proxy for convective gravity wave excitation: a study based on global gravity wave observations in the middle atmosphere, Ann. Geophys., 32, 1373–1394, doi:10.5194/angeo-32-1373-2014, http://www.ann-geophys.net/32/1373/2014/, 2014.

Jiang, J., Wang, B., Goya, K., Hocke, K., Eckermann, S., Ma, J., Wu, D., and Read, W.: Geographical distribution and interseasonal variability of tropical deep convection: UARS MLS observations and analyses, J. Geophys. Res. Atmos., 109, D03111, doi:10.1029/2003JD003756, 2004.

Kershaw, R.: Parametrization of momentum transport by convectively generated gravity waves, Q. J. Roy. Meteorol. Soc., 121, 1023–1040, doi:10.1002/qj.49712152505, http://dx.doi.org/10.1002/qj.49712152505, 1995.

Khouider, B. and Moncrieff, M. W.: Organized Convection Parameterization for the ITCZ, Journal of the Atmospheric Sciences, 72, 3073–3096, doi:10.1175/JAS-D-15-0006.1, http://dx.doi.org/10.1175/JAS-D-15-0006.1, 2015.

Kilpatrick, T. J. and Xie, S.-P.: ASCAT observations of downdrafts from mesoscale convective systems, Geophys. Res. Lett., 42, 1951–1958, doi:10.1002/2015GL063025, http://dx.doi.org/10.1002/2015GL063025, 2015.

Kim, J.-E. and Alexander, M. J.: Tropical Precipitation Variability and Convectively Coupled Equatorial Waves on Submonthly Time Scales in Reanalyses and TRMM, J. Clim., 26, 3013–3030, doi:10.1175/JCLI-D-12-00353.1, 2013.

Kim, S.-Y., Chun, H.-Y., and Baik, J.-J.: Sensitivity of typhoon-induced gravity waves to cumulus parameterizations, Geophys. Res. Lett., 34, L15814, doi:10.1029/2007GL030592, 2007.

Kim, Y.-H. and Chun, H.-Y.: Contributions of equatorial wave modes and parameterized gravity waves to the tropical QBO in HadGEM2, J. Geophys. Res. Atmos., 120, 1065–1090, doi:10.1002/2014JD022174, http://dx.doi.org/10.1002/2014JD022174, 2015.

Kim, Y.-J., Eckermann, S. D., and Chun, H.-Y.: An overview of the past, present and future of gravity-wave drag parameterization for numerical climate and weather prediction models - Survey article, Atmos.-Ocean, 41, 65–98, doi:10.3137/ao.410105, 2003.

Leena, P., Venkat Ratnam, M., and Krishna Murthy, B.: Inertia gravity wave characteristics and associated fluxes observed using five years of radiosonde measurements over a tropical station, J. Atm. Sol.-Terr. Phys., 84-85, 37–44, doi:j.jastp.2012.05.004, 2010.

Lehmann, C. I., Kim, Y.-H., Preusse, P., Chun, H.-Y., Ern, M., and Kim, S. Y.: Consistency between Fourier transform and small-volume few-wave decomposition for spectral and spatial variability of gravity waves above a typhoon, Atmos. Meas. Tech., 5, 1637–1651, doi:10.5194/amt-5-1637-2012, 2012.

Lighthill, M. J.: Waves in fluids, Comm. Pure Appl. Math., 20, 267–293, doi:10.1002/cpa.3160200204, http://dx.doi.org/10.1002/cpa.3160200204, 1967.

Lindzen, R. S.: Turbulence and Stress Owing to Gravity Wave and Tidal Breakdown, J. Geophys. Res., 86, 9707–9714, 1981.

Liu, C. and Zipser, E. J.: The global distribution of largest, deepest, and most intense precipitation systems, Geophys. Res. Lett., 42, 3591–3595, doi:10.1002/2015GL063776, http://dx.doi.org/10.1002/2015GL063776, 2015.

Marks, C. J. and Eckermann, S. D.: A three-dimensional nonhydrostatic ray-tracing model for gravity waves: formulation and preliminary results for the middle atmosphere, J. Atmos. Sci., 52, 1959–1984, 1995.

Matsuno, T.: A quasi one-dimensional model of the middle atmosphere circulation interacting with internal gravity waves, J. Met. Soc. Japan, 60, 215–226, 1982.

McIntyre, M. E.: Breaking waves and global scale chemical transport in the Earth's atmosphere, with spinoffs for the Sun's interior, Prog. of Theor. Phys., 130, 137–166, 1998.

McLandress, C.: On the importance of gravity waves in the middle atmosphere and their parameterization in general circulation models, J. Atmos. Terr. Phys., 60, 1357–1383, 1998.

McLandress, C., Alexander, M. J., and Wu, D. L.: Microwave Limb Sounder observations of gravity waves in the stratosphere: A climatology and interpretation, J. Geophys. Res., 105, 11 947–11 967, 2000.

Pitteway, M. L. V. and Hines, C. O.: The viscous damping of atmospheric gravity waves, Can. J. Phys., 41, 1935–1948, doi:10.1139/p63-194, http://dx.doi.org/10.1139/p63-194, 1963.

Pramitha, M., Venkat Ratnam, M., Taori, A., Krishna Murthy, B. V., Pallamraju, D., and Vijaya Bhaskar Rao, S.: Evidence for tropospheric wind shear excitation of high-phase-speed gravity waves reaching the mesosphere using the ray-tracing technique, Atmos. Chem. Phys., 15, 2709–2721, doi:10.5194/acp-15-2709-2015, 2015.

Preusse, P., Dörnbrack, A., Eckermann, S. D., Riese, M., Schaeler, B., Bacmeister, J. T., Broutman, D., and Grossmann, K. U.: Space-based measurements of stratospheric mountain waves by CRISTA, 1. Sensitivity, analysis method, and a case study, J. Geophys. Res., 107, doi:10.1029/2001JD000699, 2002.

Preusse, P., Ern, M., Bechtold, P., Eckermann, S. D., Kalisch, S., Trinh, Q. T., and Riese, M.: Characteristics of gravity waves resolved by ECMWF, Atmos. Chem. Phys., 14, 10 483–10 508, doi:10.5194/acp-14-10483-2014, http://www.atmos-chem-phys.net/14/10483/2014, 2014.

Ricciardulli, L. and Garcia, R. R.: The excitation of equatorial waves by deep convection in the NCAR Community Climate Model (CCM3), J. Atmos. Sci., 57, 3461–3487, 2000.

Rienecker, M. M., Suarez, M. J., Gelaro, R., Todling, R., Bacmeister, J., Liu, E., Bosilovich, M. G., Schubert, S. D., Takacs, L., Kim, G.-K., Bloom, S., Chen, J., Collins, D., Conaty, A., da Silva, A., Gu, W., Joiner, J., Koster, R. D., Lucchesi, R., Molod, A., Owens, T., Pawson, S., Pegion, P., Redder, C. R., Reichle, R., Robertson, F. R., Ruddick, A. G., Sienkiewicz, M., and Woollen, J.: MERRA: NASA's Modern-Era Retrospective Analysis for Research and Applications, J. Clim., 24, 3624–3648, doi:10.1175/JCLI-D-11-00015.1, 2011.

Rind, D., Suozzo, R., Balachandran, N. K., Lacis, A., and Russell, G.: The GISS Global Climate-Middle Atmosphere Model. Part I: Model Structure and Climatology, J. Atmos. Sci., 45, 329–370, doi:10.1175/1520-0469(1988)045<0329:TGGCMA>2.0.CO;2, http://dx.doi.org/10.1175/1520-0469(1988)045<0329:TGGCMA>2.0.CO;2, 1988.

Song, I. S. and Chun, H. Y.: Momentum flux spectrum of convectively forced internal gravity waves and its application to gravity wave drag parameterization. Part I: theory, J. Atmos. Sci., 62, 107–124, 2005.

Song, I.-S., Chun, H.-Y., and Lane, T. P.: Generation Mechanisms of Convectively Forced Internal Gravity Waves and Their Propagation to the Stratosphere, J. Atmos. Sci., 60, 1960–1980, 2003.

Trinh, Q. T., Kalisch, S., Preusse, P., Chun, H.-Y., Eckermann, S. D., Ern, M., and Riese, M.: A comprehensive observational filter for satellite infrared limb sounding of gravity waves, Atmos. Meas. Tech., 8, 1491–1517, doi:10.5194/amt-8-1491-2015, http://www.atmos-meas-tech.net/8/1491/2015/, 2015.

Wright, J. S. and Fueglistaler, S.: Large differences in reanalyses of diabatic heating in the tropical upper troposphere and lower stratosphere, Atmos. Chem. Phys., 13, 9565–9576, doi:10.5194/acp-13-9565-2013, http://www.atmos-chem-phys.net/13/9565/2013/, 2013.

Zhu, X.: A New Theory of the Saturated Gravity Wave Spectrum for the Middle Atmosphere, J. Atmos. Sci., 51, 3615–3626, 1994.

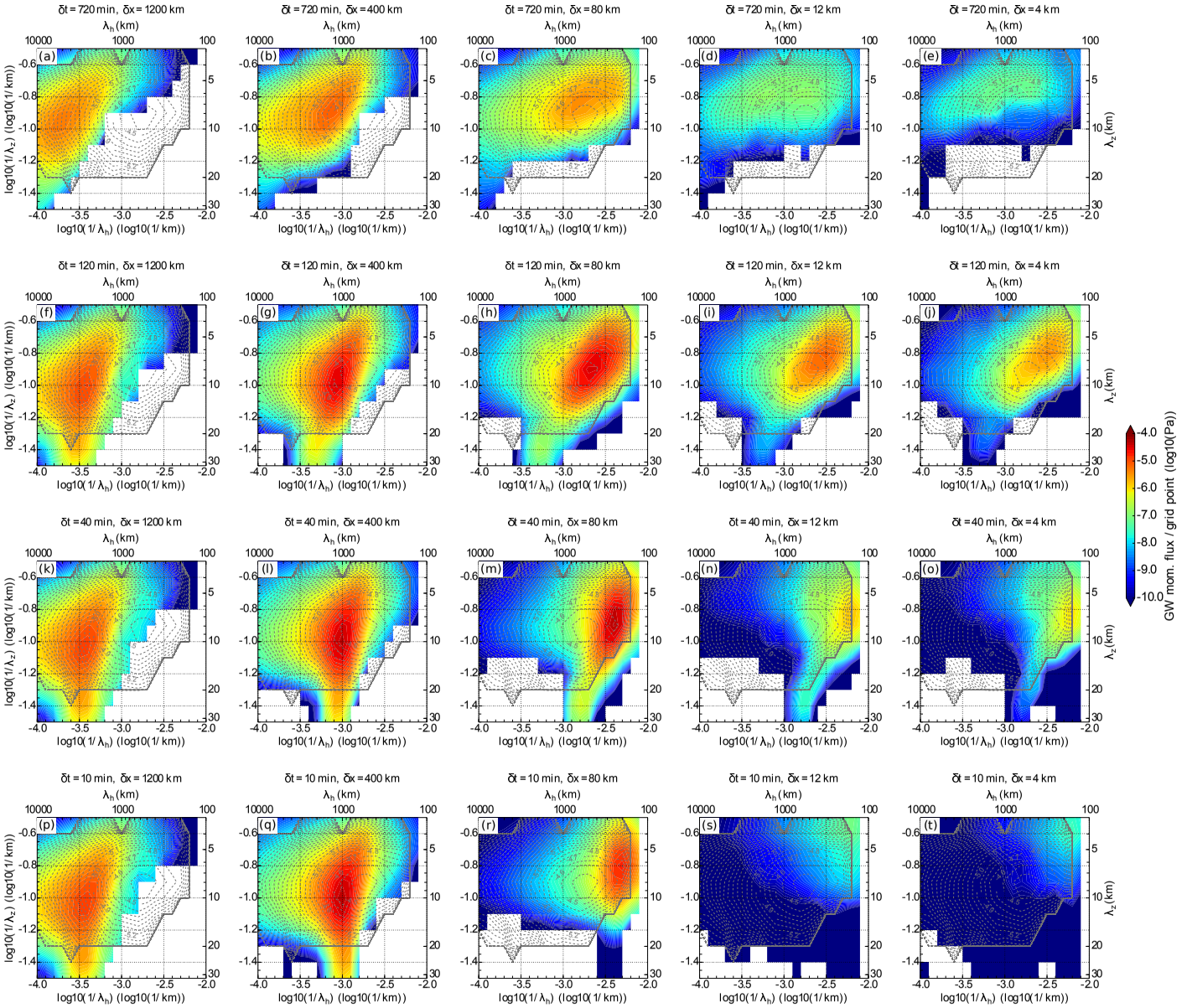

Figure 1. A systematic survey of the CGWS scheme depending on different spatial and temporal scales of the convective system for July 2006. The color code shows the simulated GWMF spectra of CGWs generated by the Yonsei CGWS scheme, propagated upward to 25 km altitude using GROGRAT and filtered according to the observational filter. The dashed contour lines show the spectrum for regions of deep convection observed by HIRDLS.

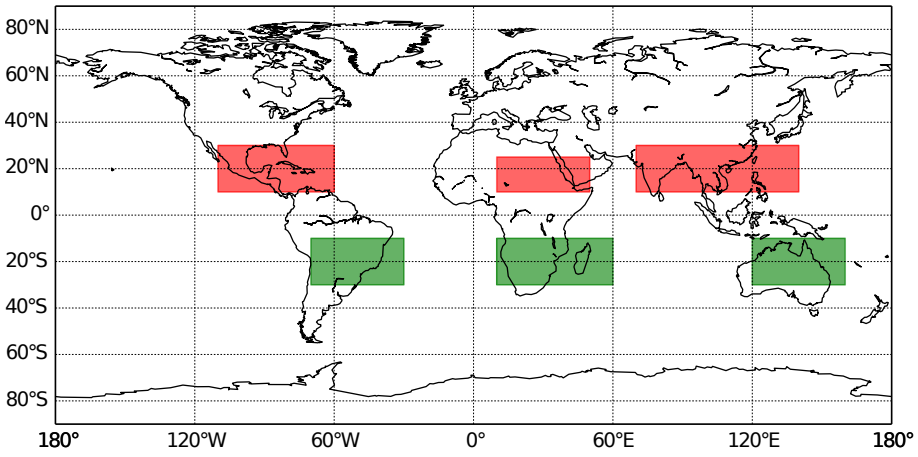

Figure 2. Regions of deep convection. For the northern hemisphere, three regions of deep convection are demonstrated by three red rectangles. For the southern hemisphere, three regions of deep convection are indicated by three green rectangles.

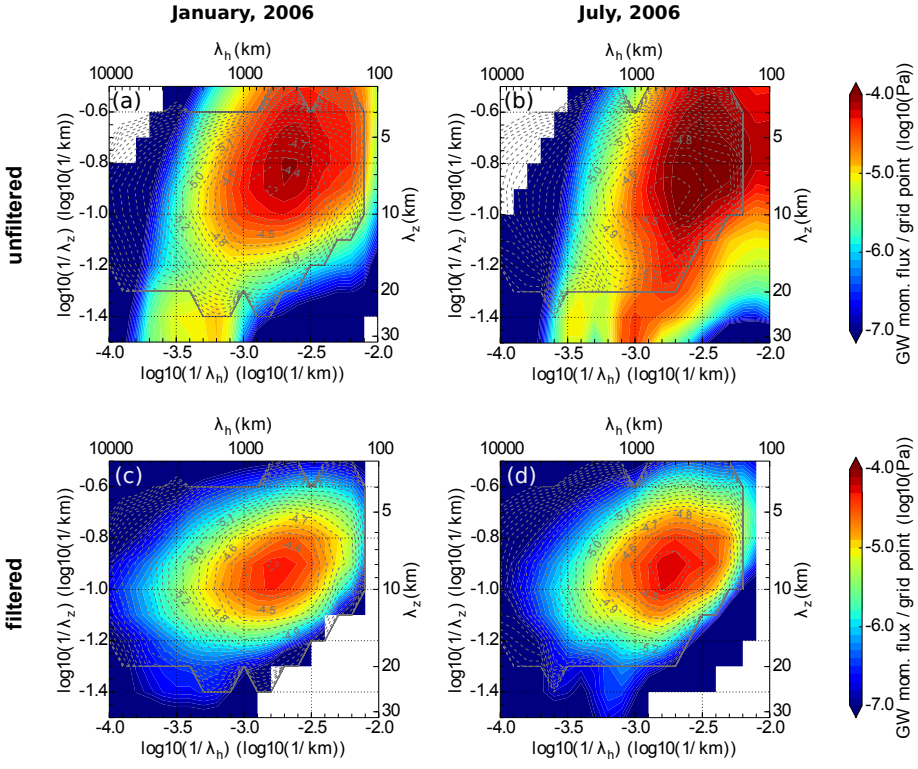

Figure 3. Unfiltered combined GW spectra of selected scale sets for (a) January 2006 and (b) July 2006 and filtered combined spectra of selected scale sets for (c) January 2006 and (d) July 2006. All spectra are shown for the altitude level of 25 km. The color code represents combined filtered simulated spectra; the dashed contour lines represent spectra observed by HIRDLS for regions of deep convection.

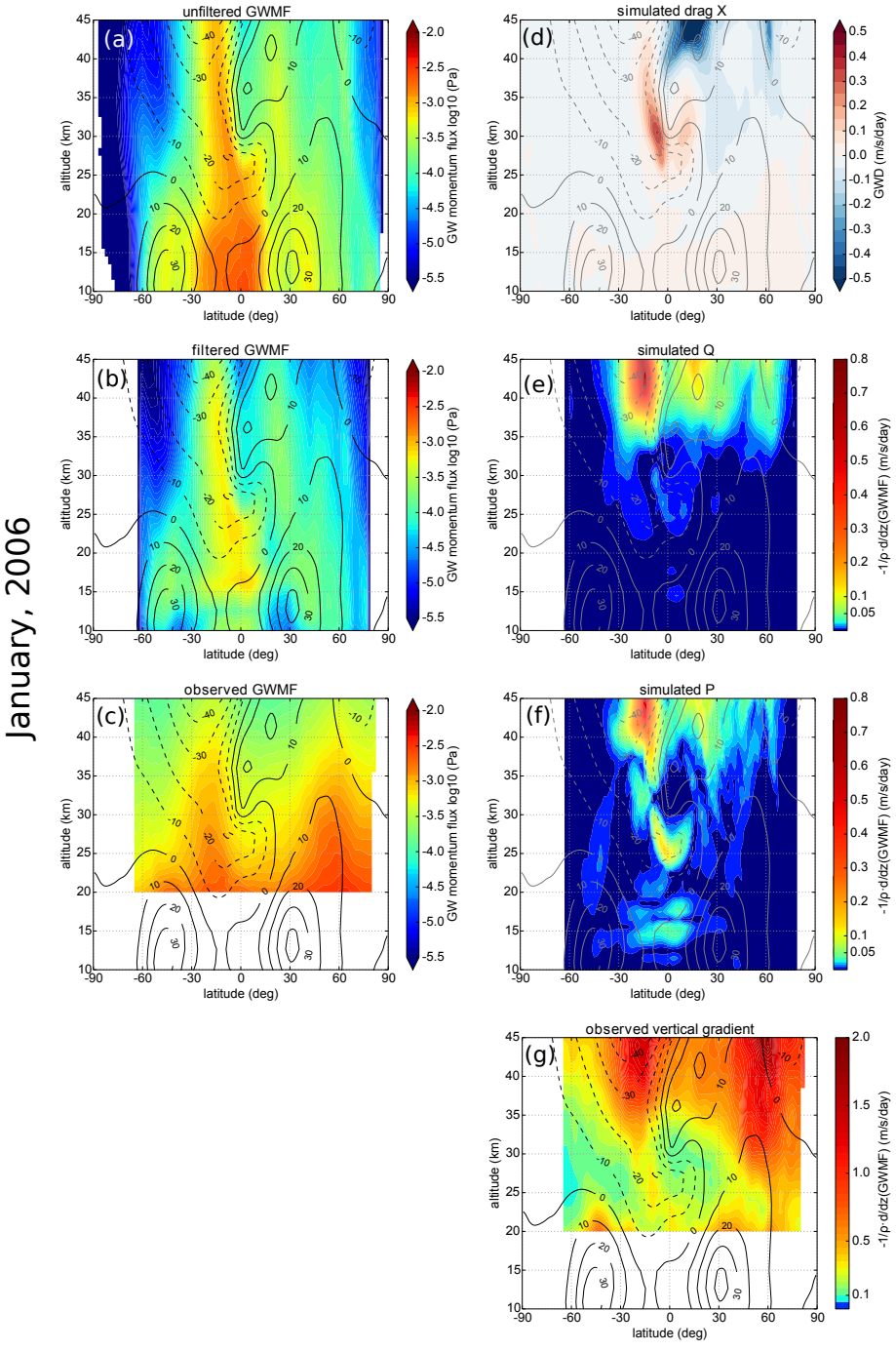

Figure 4. Comparison of simulated GWMF and its vertical gradients with observations from HIRDLS for January 2006. Panel (a) shows simulated unfiltered absolute GWMF. Panel (b) shows simulated filtered absolute GWMF. Panel (c) shows absolute GWMF observed by HIRDLS. Panel (d) shows simulated zonal GW drag. Panel (e) shows simulated vertical gradient Q. Panel (f) shows simulated vertical gradient P. Panel (g) shows observed vertical gradient of absolute GWMF from HIRDLS. Simulations were performed using MERRA data. For details see text.

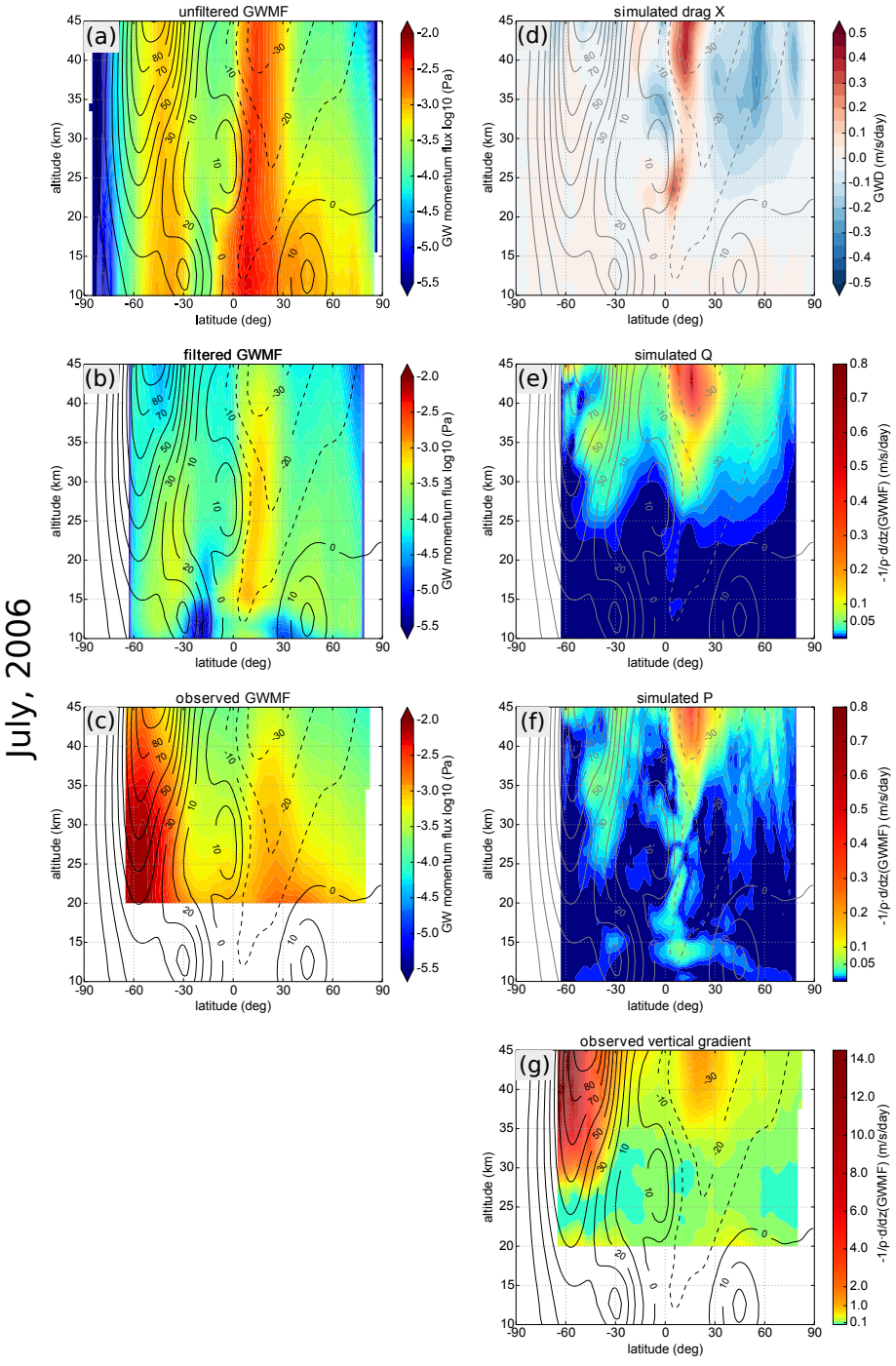

Figure 5. Comparison of simulated GWMF and its vertical gradients with observations from HIRDLS for July 2006. Panel (a) shows simulated unfiltered absolute GWMF. Panel (b) shows simulated filtered absolute GWMF. Panel (c) shows absolute GWMF observed by HIRDLS. Panel (d) shows simulated zonal GW drag. Panel (e) shows simulated vertical gradient Q. Panel (f) shows simulated vertical gradient P. Panel (g) shows observed vertical gradient of absolute GWMF from HIRDLS. Simulations were performed using MERRA data. For details see text.

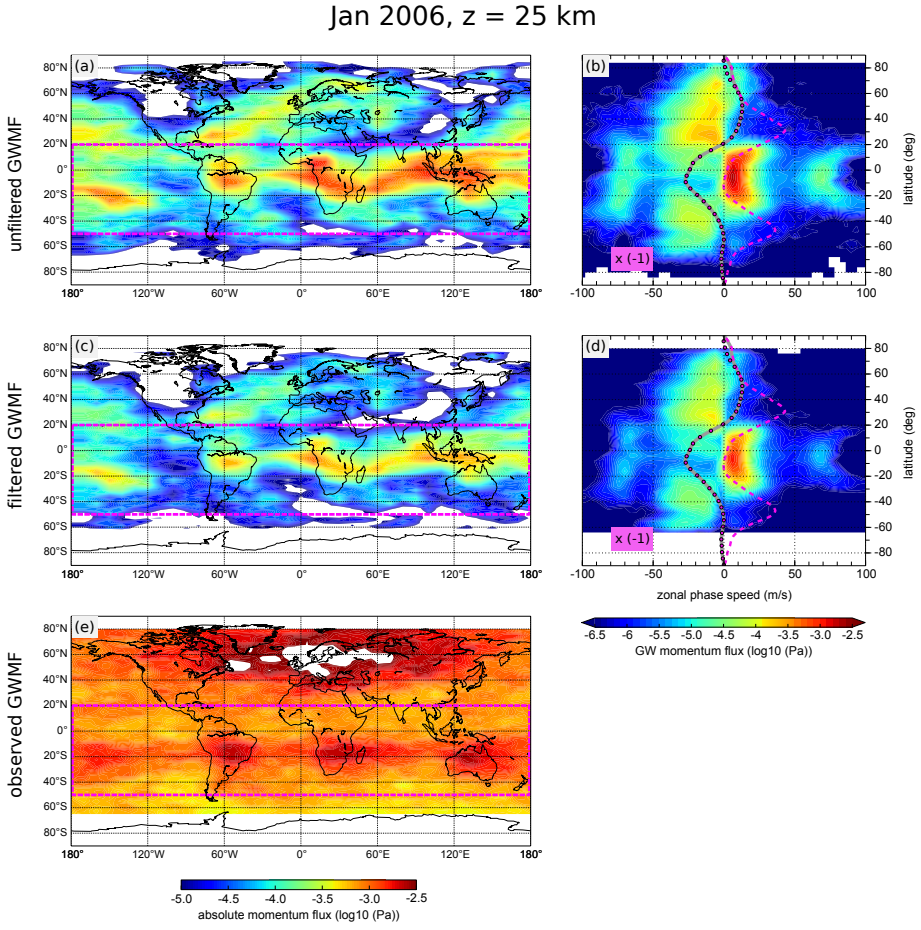

Figure 6. Horizontal distribution of (a) unfiltered absolute GWMF and (c) filtered absolute GWMF in comparison with (e) horizontal distribution of observed absolute GWMF. Panel (b) shows phase speed spectrum of unfiltered zonal GWMF (absolute values) and panel (d) shows phase speed spectrum of filtered zonal GWMF (absolute values). In phase speed spectra, GWMF values associated with negative values of phase speed (on the left-hand side) are multiplied with -1. Results are shown for January 2006 at 25 km altitude. Simulations were performed using MERRA data. For details see text.

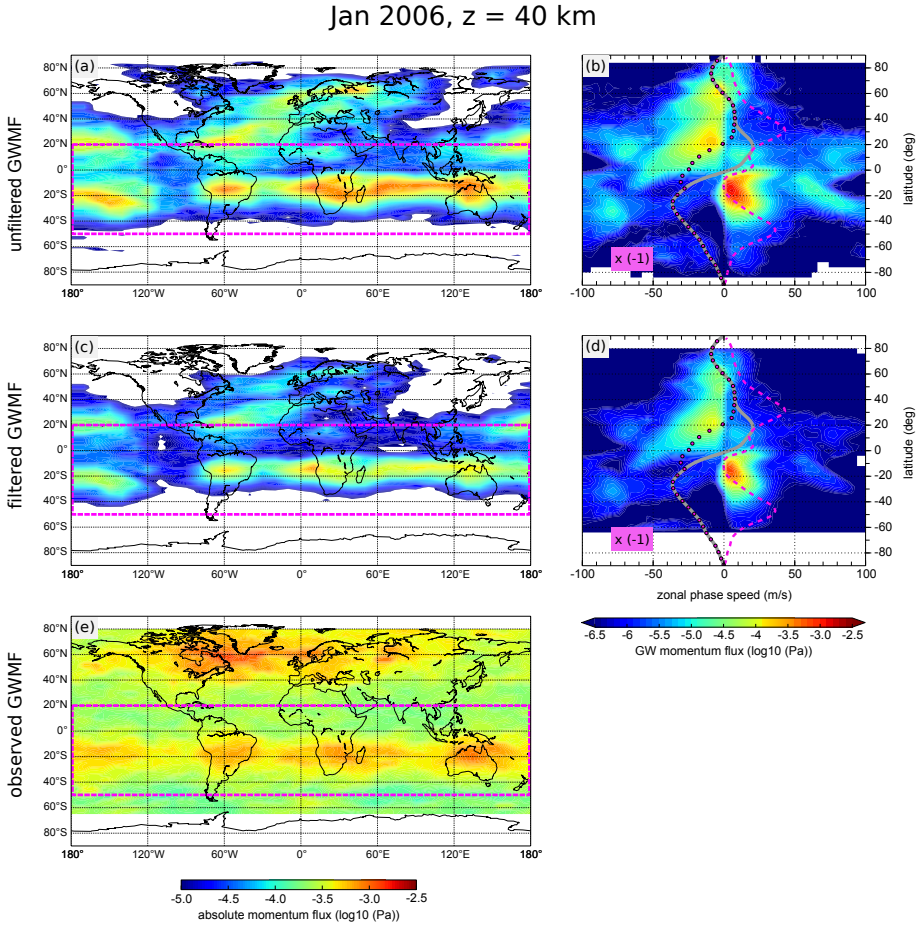

Figure 7. Horizontal distribution of (a) unfiltered absolute GWMF and (c) filtered absolute GWMF in comparison with (e) horizontal distribution of observed absolute GWMF. Panel (b) shows phase speed spectrum of unfiltered zonal GWMF (absolute values) and panel (d) shows phase speed spectrum of filtered zonal GWMF (absolute values). In phase speed spectra, GWMF values associated with negative values of phase speed (on the left-hand side) are multiplied with -1. Results are shown for January 2006 at 40 km altitude. Simulations were performed using MERRA data. For details see text.

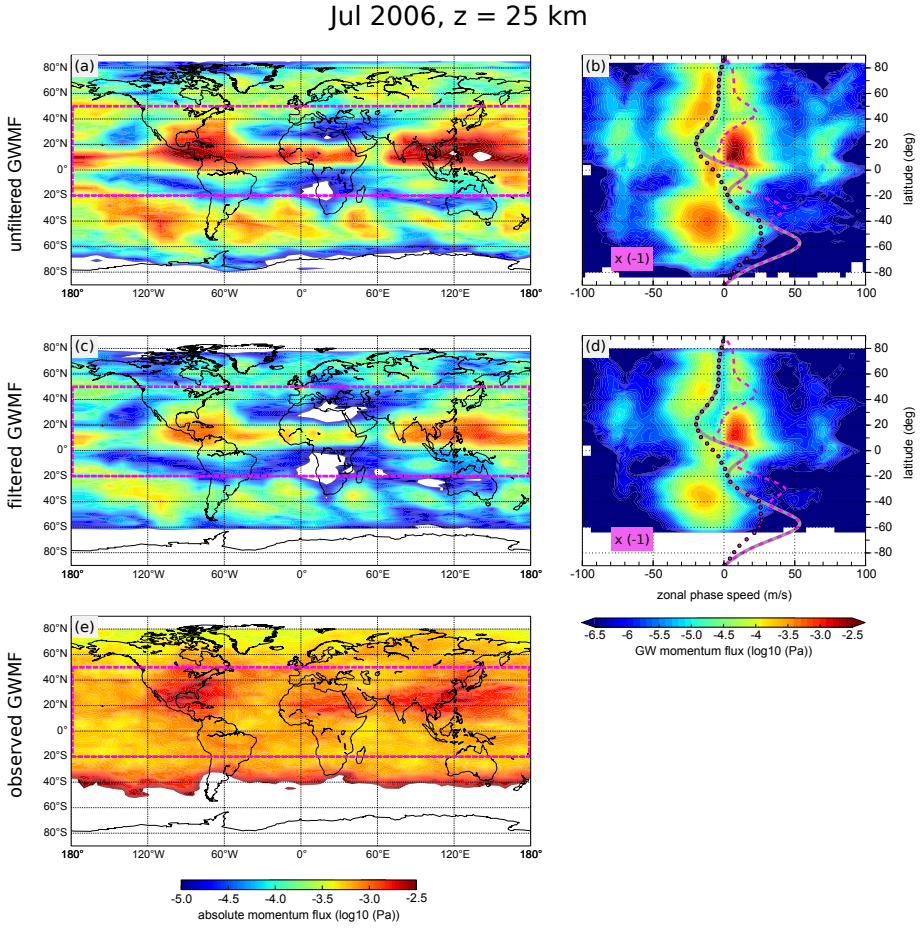

Figure 8. Horizontal distribution of (a) unfiltered absolute GWMF and (c) filtered absolute GWMF in comparison with (e) horizontal distribution of observed absolute GWMF. Panel (b) shows phase speed spectrum of unfiltered zonal GWMF (absolute values) and panel (d) shows phase speed spectrum of filtered zonal GWMF (absolute values). In phase speed spectra, GWMF values associated with negative values of phase speed (on the left-hand side) are multiplied with -1. Results are shown for July 2006 at 25 km altitude. Simulations were performed using MERRA data. For details see text.

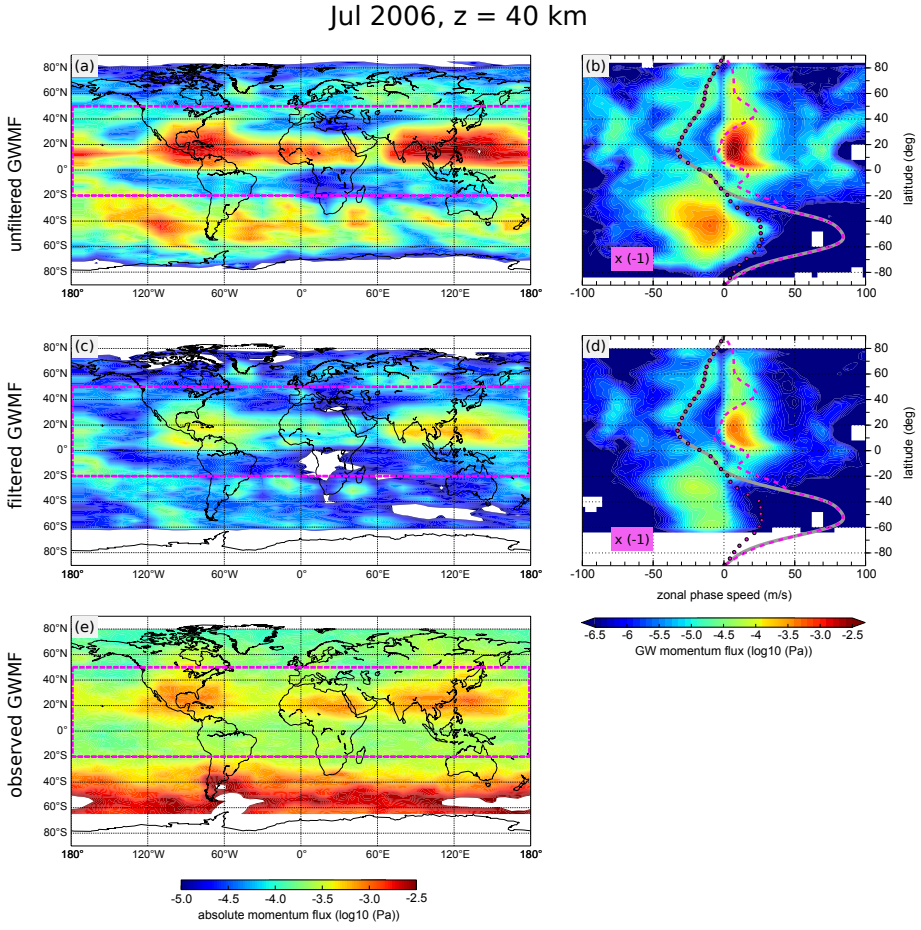

Figure 9. Horizontal distribution of (a) unfiltered absolute GWMF and (c) filtered absolute GWMF in comparison with (e) horizontal distribution of observed absolute GWMF. Panel (b) shows phase speed spectrum of unfiltered zonal GWMF (absolute values) and panel (d) shows phase speed spectrum of filtered zonal GWMF (absolute values). In phase speed spectra, GWMF values associated with negative values of phase speed (on the left-hand side) are multiplied with -1. Results are shown for July 2006 at 40 km altitude. Simulations were performed using MERRA data. For details see text.

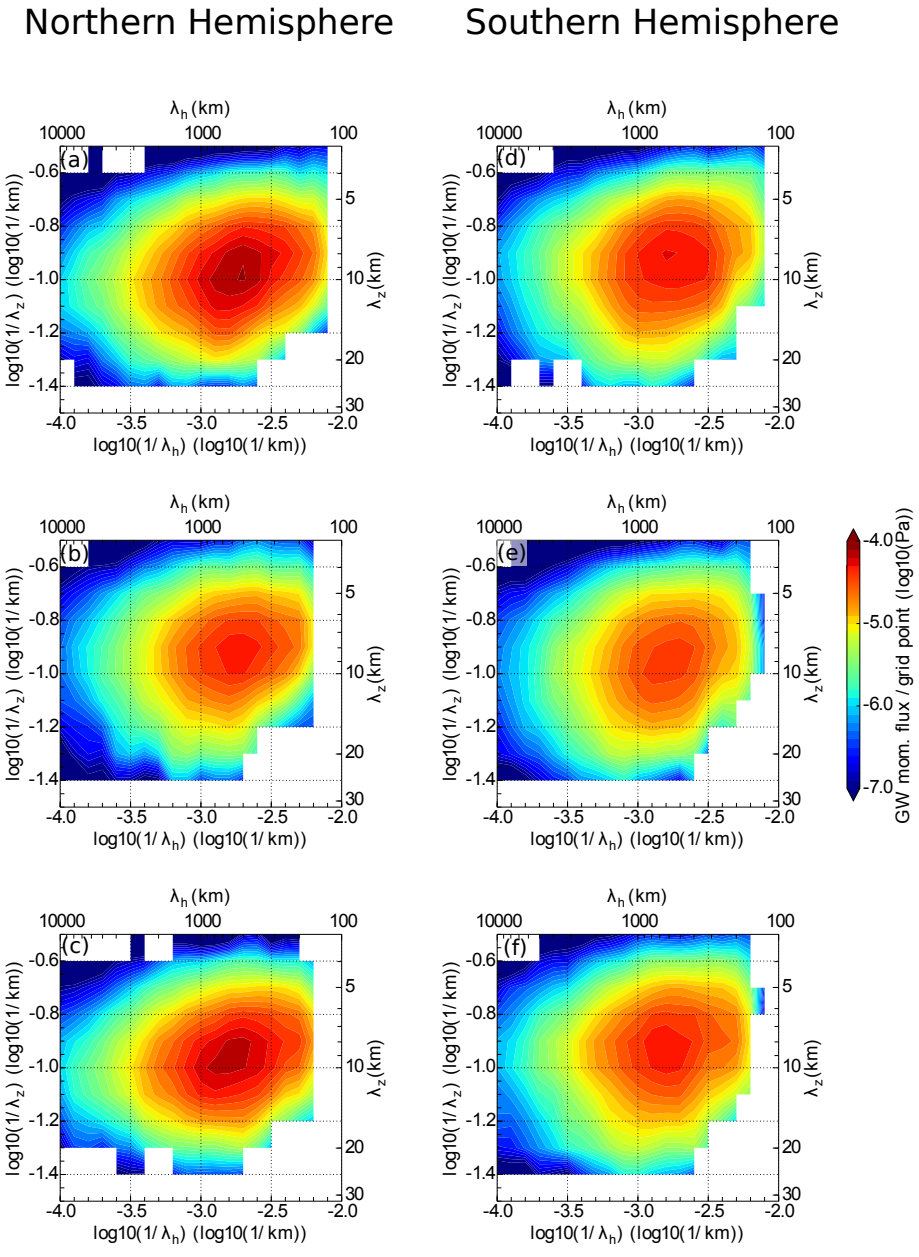

Figure A1. Observed spectra for different hemispheres for 3 consecutive years. Panels (a) (b) (c) show spectra averaged for boreal summer (June-August) for 2005, 2006, 2007 respectively; panels (d), (e), (f) show spectra averaged for austral summer (December-February) for 2005/6, 2006/7, 2007/8. All spectra are averaged over three regions of deep convection of each hemisphere as shown in Fig. 2.

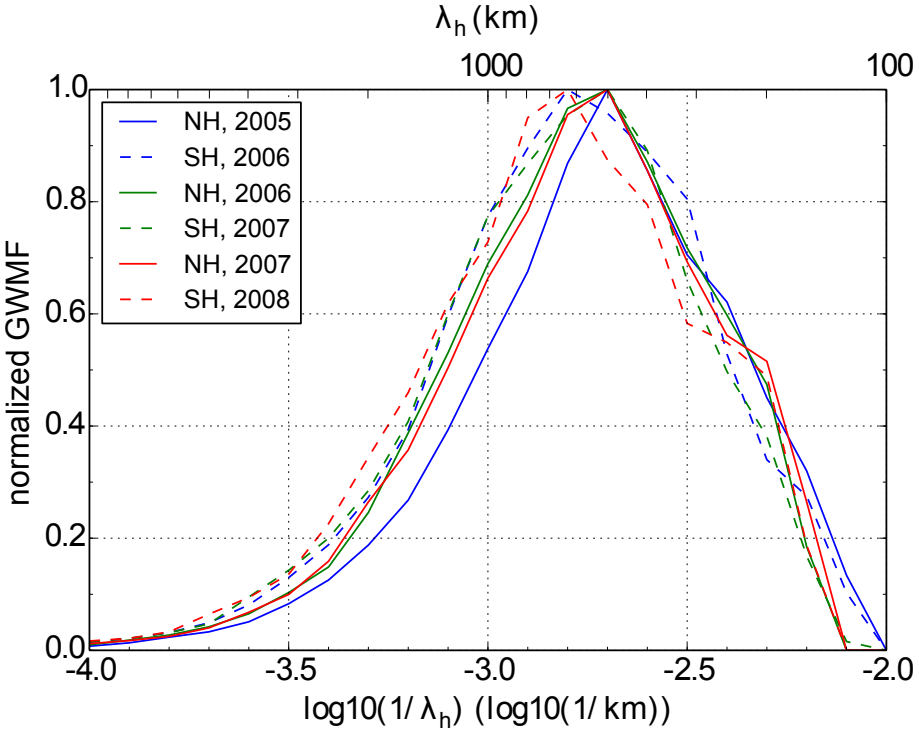

Figure A2. Observed normalized GWMF spectra at vertical wavelength $\lambda_z = 9$ km for different hemispheres for 3 consecutive years. Solid blue, green, red lines show spectra averaged for boreal summer (June-August) for 2005, 2006, 2007 respectively. Dashed blue, green, red lines show spectra averaged for austral summer (December-February) for 2005/6, 2006/7, 2007/8.

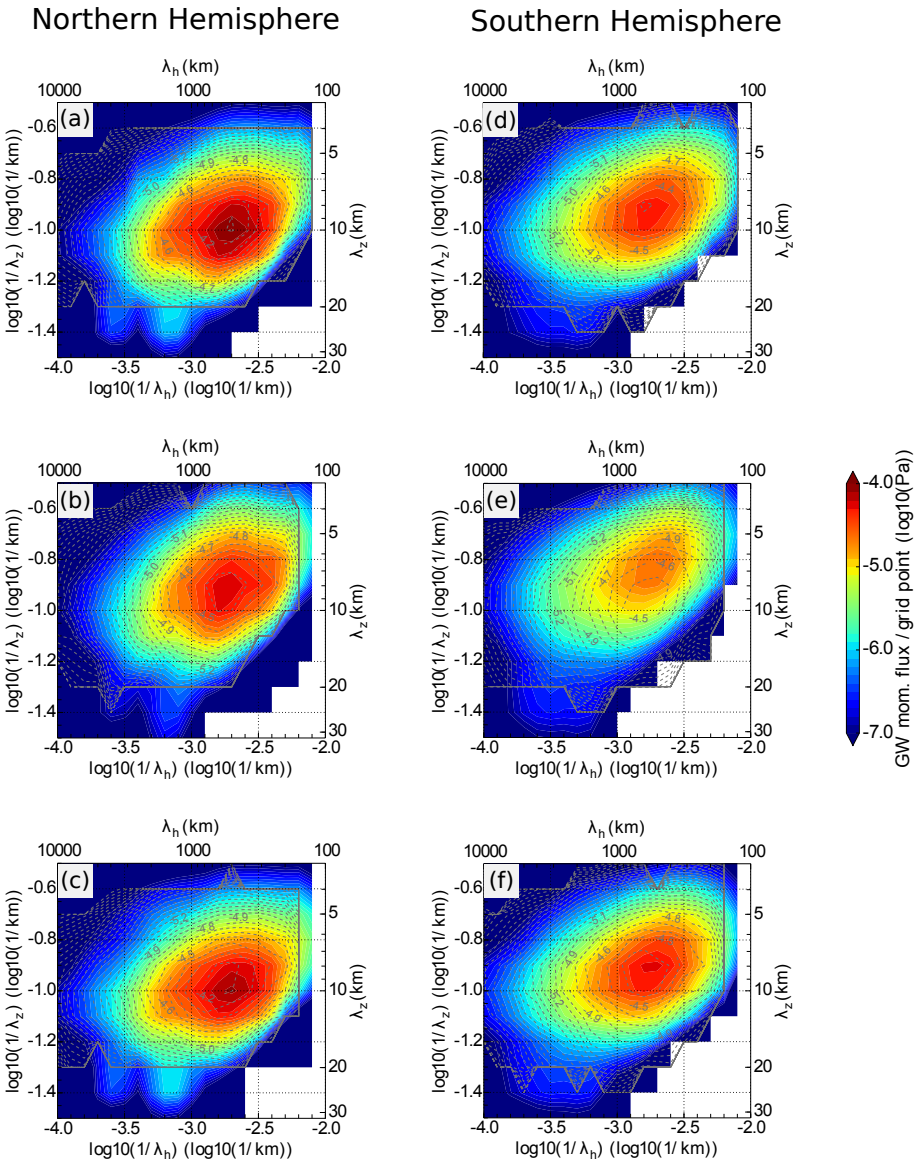

Figure A3. Filtered simulated GWMF spectra for different hemispheres for 3 consecutive years. Panels (a) (b) (c) show spectra for July 2005, 2006, 2007 respectively; panels (d), (e), (f) show spectra for January 2006, 2007, 2008. All spectra are averaged over three regions of deep convection of each hemisphere as shown in Fig. 2

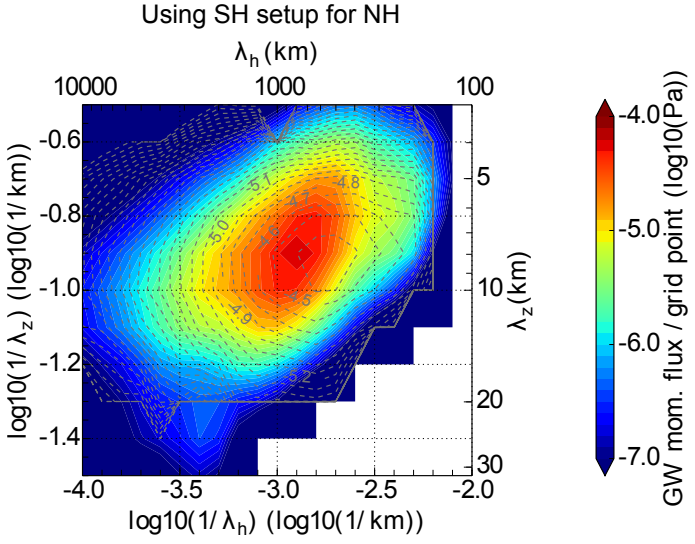

Figure A4. Filtered simulated GWMF spectra for Northern Hemisphere (July) 2006, run by using the set of scales selected for Southern Hemisphere (January 2006).

Table 1. Surveyed and selected spatial and time scales (δx, δt) as well as intermittency factor (ζ) for the Yonsei CGWS scheme.

Scales used for surveying		Selected scales for January			Selected scales for July		
δx (km)	δt (min)	δx (km)	δt (min)	ζ	δx (km)	δt (min)	ζ
4	**10**	80	240	1.0	40	80	1.0
8	20	120	120	0.4	160	100	1.0
12	**40**	200	150	0.4	250	240	1.0
25	80	250	360	0.7			
40	**120**						
80	240						
120	360						
250	**720**						
400							
800							
1200							